PLASMONIC FIELD EFFECTS OF SILVER NANOPARTICLE MONOLAYERS ON POLY(PHENYLENE ETHYNYLENE) FLUORESCENT POLYMERS OF DIFFERENT CHAIN LENGTH

A Thesis
Presented to
The Academic Faculty

by

Adam James Poncheri

In Partial Fulfillment
of the Requirements for the Degree
Master of Science in Chemistry
School of Chemistry and Biochemistry

Georgia Institute of Technology
August 2011

PLASMONIC FIELD EFFECTS OF SILVER NANOPARTICLE MONOLAYERS ON POLY(PHENYLENE ETHYNYLENE) FLUORESCENT POLYMERS OF DIFFERENT CHAIN LENGTH

Approved by:

Dr. Mostafa A. El-Sayed, Advisor
School of Chemistry and Biochemistry
Georgia Institute of Technology

Dr. Lawrence A. Bottomley
School of Chemistry and Biochemistry
Georgia Institute of Technology

Dr. Paul H. Wine
School of Chemistry and Biochemistry
Georgia Institute of Technology

Date Approved: May 16, 2011

to Kristin Leigh

ACKNOWLEDGEMENTS

I would like to thank my advisor Professor Mostafa El-Sayed for the opportunity to work in his distinguished group and for his continued support, which I know will extend well beyond my years at Georgia Tech. It was his guidance and the people within the LDL group that allowed me to accomplish the works presented herein. Within the group I would like to especially thank Mr. Erik Dreaden, Mr. Steven Hayden, Ms Megan Mackey, Ms. Rachel Near, and Dr. Chun-wan Yen for aiding, and sometimes pushing, me through the entirety of my Georgia Tech career. I would also like to thank Professor Lawrence Bottomley and Professor Paul Wine for serving on my thesis committee and providing additional guidance and support.

Personally, I must thank and acknowledge my wife and my parents. Without their love, support, and their personal sacrifices, I would not be in such a position to succeed. I would also like to thank my friends, old and new, for being that "familiar place" for me to go when life in graduate school was overwhelming. Even though I was focused on the work in front of me and I was not always the best at keeping up with them, they kept up with me.

Thank you all.

TABLE OF CONTENTS

LIST OF FIGURES

LIST OF SYMBOLS

α	Dipole Polarizability
C	Plasmonic Enhancement Factor
ε	Dielectric Permittivity of the material
ε_m	Dielectric Permittivity of the Medium
I	Lamp Intensity
λ_{max}	Peak Maximum
n	Polymer Repeat Units
σ	Fraction of the Area of Excitation that Contains Nanoparticle Interpaticle Distances at or Below the Critical Distance
V	Volume of the Nanoparticle

LIST OF ABBREVIATIONS

2D	Two Dimensions (or Two-Dimensional)
3D	Three Dimensions (or Three-Dimensional)
ACS	American Chemical Society
AFM	Atomic Force Microscopy (or Microscope)
AgNC	Silver Nanocube
AgNCs	Silver Nanocubes
CW	Continuous Wave
DDA	Discrete Dipole Approximation
DMF	Dimethylformamide
EBL	Electron Beam Lithography
EG	Ethylene Glycol
EM	Electromagnetic
ES	Excited State
Fl	Fluorescence
FWHM	Full Width at Half Maximum
GPC	Gel Permeation Chromatography
GS	Ground State
IPD	Interparticle Distance
LB	Langmuir-Blodgett
LSPR	Localized Surface Plasmon Resonance
MeOH	Methanol
MCP-PMT	Microchannel Plate-Photomultiplier Tube

MW	Molecular Weight
NIR	Near-Infrared
NSL	Nanosphere Lithography
PDI	Polydispersity Index
PEG	Polyethylene Glycol
PPE	Poly(phenylene ethynylene)
PPE15	Poly(phenylene ethynylene) Containing 15 Repeat Units
PPE25	Poly(phenylene ethynylene) Containing 25 Repeat Units
PPE36	Poly(phenylene ethynylene) Containing 36 Repeat Units
PPE/AgNC	PPE Monolayer Deposited onto AgNC Monolayer
ppm	Parts per Million
PTFE	Polytetrafluoroethylene
PVP	Polyvinylpyrrolidone
SD	Standard Deviation
SEM	Scanning Electron Microscopy (or Microscope)
SERS	Surface Enhanced Raman Scattering
SP	Surface Pressure
SPR	Surface Plasmon Resonance
TEM	Transmission Electron Microscopy (or Microscope)
THF	Tetrahydrofuran
UV	Ultraviolet

SUMMARY

The literature on nanomaterials has been flooded with new shapes, sizes, and compositions of nanostructures. The process of developing and characterizing these particles has been broadly accomplished and many interesting and promising properties have been revealed for application in current and developing technologies. In particular, the phenomenon of surface plasmon resonance seen in metallic gold and silver nanoparticles has drawn substantial interest. It has been established that the electromagnetic fields surrounding plasmonic particle surfaces can influence the properties of nearby systems, causing them to experience effects such as enhanced absorption and emission of light or drastically increased conductivity. For this reason, plasmonic nanoparticles are being applied to an endless number of applications for new materials.

This thesis investigated the effects of silver nanocube (AgNC) arrays on the photophysical properties of poly(paraphenyleneethynylene) (PPE) fluorescent polymers, a particularly relevant material to the applications of organic-electronics. AgNCs were selected because of their particularly strong plasmonic field, which is enhanced at the sharp features of the cubes. The PPE polymer is an exceptionally fluorescent conjugated polymer that often serves as a building block for polymer-based sensing applications. By monitoring the absorption and emission of the PPE polymer, a better understanding of plasmonic effects on this polymer system was obtained. Compression of the monolayer of AgNCs on the surface of a Langmuir-Blodgett trough can be used for control of

interparticle distance and, thus, the plasmon field intensity felt by an adsorbed layer of PPE polymer.

In the Chapter 4, PPE (n = 15) emission was monitored as a function of the AgNC plasmonic field. A two-photon process was found to explain the unusual increase then decrease of the fluorescence intensity. This observation was attributed to exciton-exciton annihilation processes within the polymer. The annihilation process is initiated by large enhancements of the polymer absorption rate when plasmonic fields are at their highest (when the AgNCs are compressed to short interparticle distances).

In chapter 5, the optical properties of PPE polymers as a function of their chain length and the AgNC density were examined. A simple study was conducted to consider the conformational/geometrical effects on PPE that were caused by the deposition of PPE onto the AgNC topography. In this study, the structure of the absorption and emission profiles were evaluated and used as evidence of polymer interchain interactions, planarization, and even the potential generation of oligomeric species through breaking of conjugation.

Fundamental interactions between materials must be evaluated and optimized prior to their use in devices. This thesis serves to shed a little bit of light on the interaction of a well-defined plasmonic particle with a conjugated polymer. The Langmuir-Blodgett technique serves as a critical tool in applying these colloidally produced nanoparticles to 2D arrays in practical applications. The observation of exciton-exciton annihilation at low-energy excitation is an entirely new phenomenon that was initiated by the plasmonic properties of metal nanoparticles. It is the hope of the author

that the results contained herein can aide in the use of plasmonic nanoparticles in future devices.

CHAPTER 1

INTRODUCTION

Abstract

Metallic nanoparticles have been used, albeit unknowingly, for thousands of years. This chapter introduces plasmonic nanoparticles from their age-old uses, to their actual discovery, and then to the present day fundamental science that has allowed this class of materials to spark a scientific and materials-application revolution. Manipulation of the surface plasmon resonance and the resulting electromagnetic fields are the focus of much of the research presented herein. Generation of new nanoparticle shapes and coupling of electromagnetic fields to enhance the properties of nanoparticles for specific applications are the current and future goals of the field. The last section of this chapter will discuss some of those practical applications.

1.1 A Brief Introduction to 'Nano'

The field of nanotechnology has been rapidly evolving in the past decade. The number of journal publications concerning "nano" have increased by nearly an order of magnitude since 1999 (Figure 1.1).[1] This progress has been fueled by improved manufacturing capabilities that extend micro-fabricating techniques to the nano- regime. It has also been fueled by the incorporation of new materials into nano-scale devices compared to those conventionally used in the semiconductor industry.[2-3] The immediate payoff is smaller transistors, which equate to greater a density of transistors and yield higher performance computer chips. The development of materials-fabrication techniques for nanometer dimensions has also marked a gateway to a new class of materials. The surge in research interest and, as a result, publications (Figure 1.1) is not just a simple progression of Moore's Law into a new size regime. It is due the discovery of vastly different physical and chemical properties of these new nanoscale materials compared to their bulk counterparts. The field of nanotechnology now incorporates physics, chemistry, and materials science. It has applications in numerous surrounding fields. These will only continue to grow as new materials are characterized and phenomena discovered.

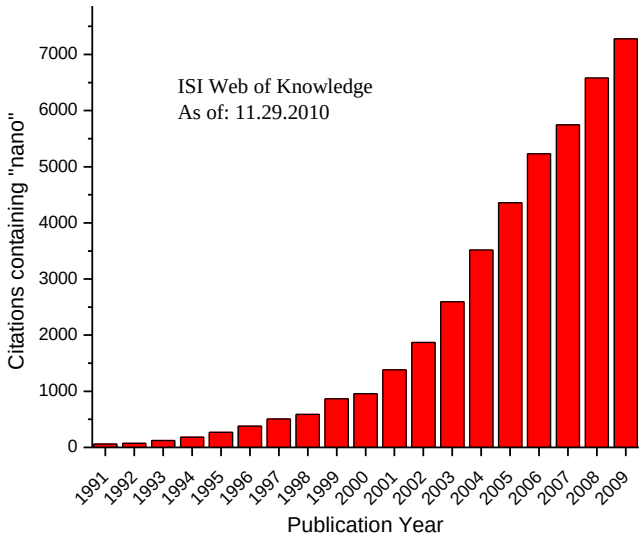

Figure 1.1: ISI Web of Knowledge search showing increase in the appearance of the term "nano" in journal article titles from 1991 to 2009. Data retrieved 11.29.2010.

Although the focus of the scientific community has only recently centered on "nano," materials, they are not new to this world. In Michael Faraday's 1857 lecture to the Royal Society in London, he discusses his findings and interest in the optical properties of colloidal gold, which was known as "ruby gold" for its vibrant color.[4] Long before Faraday's studies of gold, medieval artisans had been unknowingly creating nanoparticles when utilizing gold for pigmentation of stained glass windows and ceramics. One of the most famous examples of this practice is the Lycurgus Cup, a Roman artifact in which the glass exhibits dichroic behavior (Figure 1.2). This unique effect occurs because of the metallic nanoparticles that are incorporated into the glass, which scatter green light when illuminated from the outside and transmit red light when illuminated from the inside.[5] Although Faraday was not aware of the size of the colloidal gold with which he was working, he speculated that the ruby color of gold was the result

of the particle size approaching the wavelength of light. According to his experimental observations, he believed that the systematic variation of particle size could result in an observable effect.[4] Ancient pottery, the Lycurgus Cup, and Faraday's ruby gold samples, serve as important reference pointes in our evolving understanding of these unique materials and their properties.

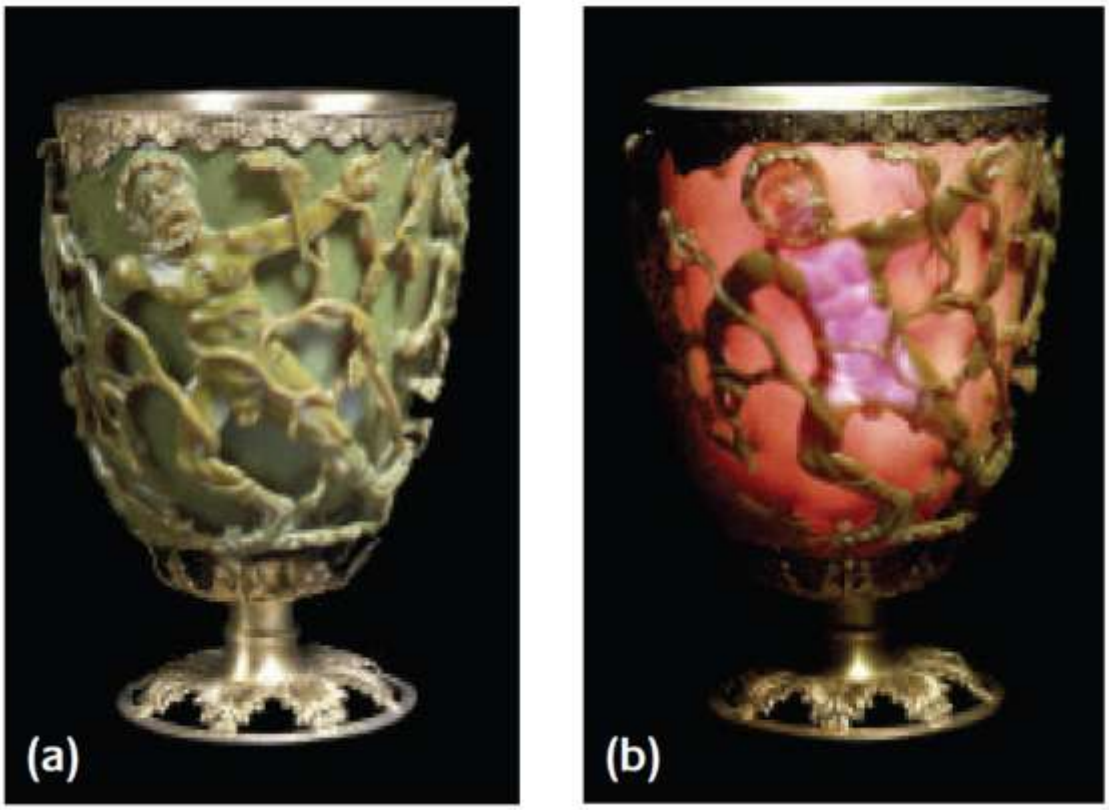

Figure 1.2: The Lycurgus Cup as illuminated from the outside (A) and the inside (B), demonstrating scattered (green) and transmitted light (red), respectively.[5]

1.2 Surface Plasmon Resonance in Metallic Nanoparticles

1.2.1 Electromagnetic Field and Optical Properties

Roughly fifty years after Michael Faraday's lecture, a German scientist named Gustav Mie proposed a theory that explains why spherical particles of different size did

indeed exhibit varied colors. By solving Maxwell's equations, he was able to predict the optical properties of spherical metallic nanoparticles and elucidate factors that contribute to their intriguing behavior.[6-7] The presence of strong absorption and scattering in the visible region is one of the most interesting features of metallic nanoparticles. These properties are the result of the localized surface plasmon resonance (LSPR), a collective oscillation of the surface electrons that occurs when light interacts with a particle at its' resonant frequency (Figure 1.3).

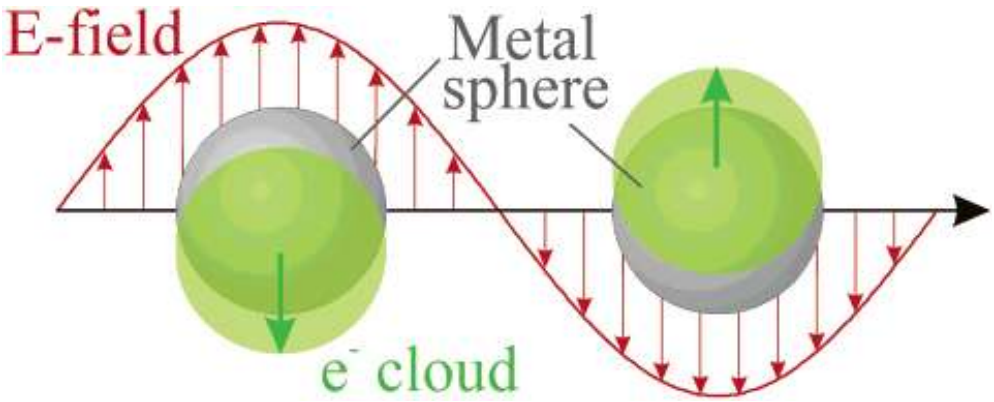

Figure 1.3: Illustration of the localized surface plasmon resonance, showing the polarization of the particle upon interaction with a resonant electromagnetic wave.[8]

In an LSPR, the rapidly oscillating electrons are associated with the production of very strong electromagnetic fields in the immediate vicinity of the nanoparticle. These fields are known to affect the properties of other materials and are of great interest. Examples of a portion of those effects on other systems will be discussed herein. Many materials of a large range of sizes can exhibit a surface plasmon. However, it is the exceptionally small size and dielectric properties of metallic nanoparticles that allow them to overcome the dominant bulk properties and produce electromagnetic enhancements orders of magnitude larger than the incident field.[9-11]

The wavelengths at which resonance occurs can be manipulated by altering the size, shape, dielectric of the particle, and dielectric of the environment surrounding the particle. Each of these aspects influences the polarizability, α, or how easily the electrons move through and away from the crystal lattice. Mie Theory was used to develop Equation 1.1, which describes these critical factors mathematically for a spherical particle. In Equation 1.1, ε and ε_m are the frequency dependent dielectric permittivity of the particle and the media, respectively. V is the volume of the particle, and the pre-factor (2 in the case of a sphere) is based on the shape of the particle. The unique characteristic of metals that makes enhanced plasmonic resonance possible is that their dielectrics become negative in certain frequency ranges. It can be seen in Equation 1.1 that at the condition where the dielectric of the metal nears $-2\varepsilon_m$, the denominator will approach zero, which results in an infinitely large dipolar polarizability. Therefore, LSPRs occur, or are resonant, at the frequencies at which $\varepsilon = -2\varepsilon_m$. For many metals, this occurs within the visible region of the electromagnetic spectrum, resulting in many vivid colors, as observed by Faraday, and unique optical spectra, as predicted by Mie.

Equation 1.1: $$\alpha = \left(\frac{\varepsilon - \varepsilon_m}{\varepsilon + 2\varepsilon_m} \right) V$$

The great versatility of metallic nanoparticles comes from the ability to fine tune the physical and optical properties for study and application alike.[10,12-15] Figure 1.4 shows the progression of color from red to blue-violet as the size of gold nanospheres is increased. Metallic nanoparticles can also be formed in a wide range of shapes (spheres,[16] rods,[17] cages,[18] cubes,[19-20] etc.), which in turn gives rise to an even wider range of spectral

properties. Nonsymmetric shapes and particles with varied aspect ratios and/or sharp features, can interact with light differently based on orientation (such as perpendicular and parallel excitation of the particle). This can result in multiple dipolar resonance peaks and even higher-order multipolar resonance peaks that constitute more complex movement of electrons within the particle.

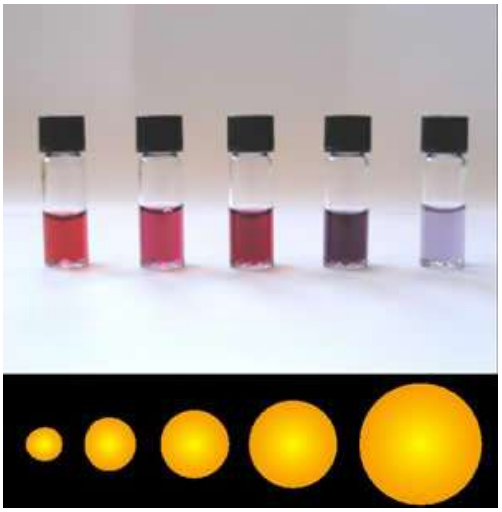

Figure 1.4: Qualitative image showing the change in solution color as the size of the gold nanosphere is increased from left to right.[21]

1.2.2 Plasmonic Coupling

The interaction of plasmonic particle pairs and clusters is of interest because the electric fields of these particles have been observed to influence neighboring systems. Optimizing these fields and controlling their effect on external systems can be accomplished through interparticle interactions. These interactions are known as nanoparticle coupling and occur when two or more nanoparticles are brought into close proximity and their surface plasmons interact to produce regions of enhanced field intensity between the particles. A characteristic red-shift in the LSPR bands is observed

as the energy of the oscillation decreases.[22-25] Hao & Schatz report the calculated electric field enhancement to be 3500 times the incident field intensity for a single particle and 53,000 times the incident field intensity between the tips of prism-shaped nanoparticle pairs (Figure 1.5).[26] The extraordinary enhancement of plasmonic fields at sharp features has been termed the "lightning rod" effect. This effect occurs at sharp features of the nanoparticle because there are very few adjacent atoms surrounding corner atoms compared to edge atoms. The lack of surrounding atoms results in little restoring force acting on the electron cloud and a greater free-electron environment, which leads to the production of larger fields. A significant amount of research has been conducted in order to understand, optimize, and make use of this enhancement through various arrangements particle arrays. Electron-beam and nanosphere lithography have been used extensively to fabricate and arrange two-dimensional metal nanoparticles in order to study the interparticle distance dependence of coupled plasmon fields.[22-24,27-28]

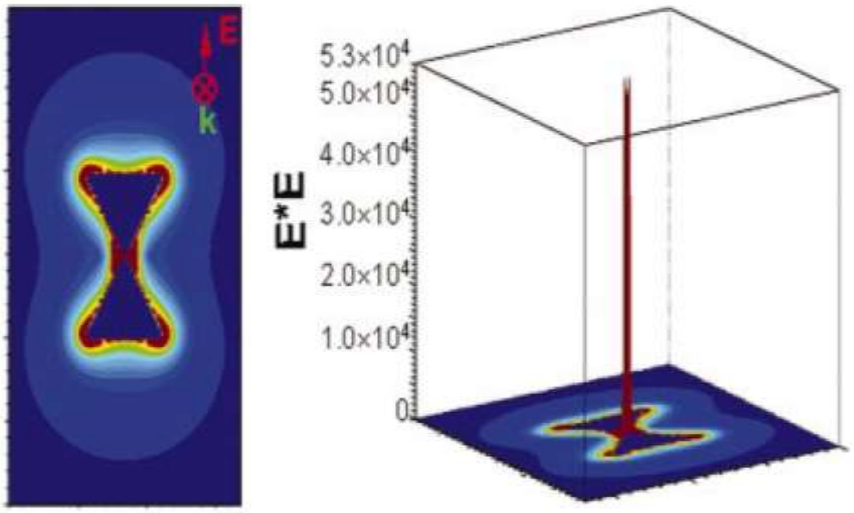

Figure 1.5: DDA models of dimer coupling of prism nanoparticles. The color contour map shows the enhancement of the incident EM field at the tips of the nanoparticles.[26]

1.3 Applications and Effects of Plasmonic Nanoparticles

Metallic nanoparticles have been used in wide-ranging applications such as catalysis,[16] sensing,[29-31] drug delivery,[32-33] and the potential diagnosis & in-vivo treatment of cancer.[34-36] In many applications of metallic nanoparticles, the plasmon field leads to an enhancement in the radiative and/or non-radiative properties of nearby electronic systems. The near-field effects can increase absorption and scattering processes by enhancing the electromagnetic field of the resonant exciting light. Surface Enhanced Raman Spectroscopy (SERS) results from this near-field plasmonic amplification of the Raman scattering spectrum of adsorbed molecular systems. Enhanced Rayleigh scattering by plasmonic fields is now used in dark-field scattering for medical diagnosis. Additionally, fluorescence of nearby molecules can be enhanced at distances from the surface that are large enough to minimize electron transfer quenching mechanisms (~5 nm), but close enough to feel the surface plasmon near-fields of the nanoparticles (~2 times the particle diameter). The near-field plasmonic effects on non-radiative processes have also been demonstrated in studies within our group. These include studies on the non-radiative electronic relaxation in semiconductor CdTe-Au core-shell nanorods,[37] effects on the rates of retinal photo-isomerization[38] and its proton pump process in the photosynthetic system of bacteriorhodopsin. In most of these systems, the mechanisms that are involved are found to be the result of large enhancements of the radiative transitions in resonance with the plasmonic frequency.

1.4 References

(1) Thomson Reuters: 2010.

(2) Moore, G. E. Cramming more components onto integrated circuits. *Electronics* **1965**, *38*, 114-117.

(3) Excerpts from A Coversation with Gordon Moore: Moore's Law. Video Transcript. 2005.

(4) Faraday, M. The Bakerian Lecture: Experimental Relations of gold (and Other Metals) to Light. *Philosophical Transactions of the Roayl Society of London* **1857**, *147*, 145-181.

(5) Freestone, I.; Meeks, N.; Sax, M.; Higgitt, C. The Lycurgus Cup- A Roman nanotechnology. *Gold Bulletin* **2007**, *40*, 270-277.

(6) Mie, G. Articles on the optical characteristics of turbid tubes, especially colloidal metal solutions. *Annals of Physics* **1908**, *25*, 377-445.

(7) Bohren, C. F.; Huffman, D. R. *Absorption and Scattering of Light by Small Particles*; Wiley Science: New York, 1983.

(8) Kelly, K. L.; Coronado, E.; Zhao, L. L.; Schatz, G. C. The Optical Properties of Metal Nanoparticles: The Influence of Size, Shape, and Dielectric Environment. *J. Phys. Chem. B* **2003**, *107*, 668-677.

(9) Kerker, M. The Optics of Colloidal Silver: Somethign Old and Something New. *J. Colloid Interface Sci.* **1985**, *105*, 297-314.

(10) Link, S.; El-Sayed, M. A. Shape and size dependence of radiative, non-radiative and photothermal properties of gold nanocrystals. *Int. Rev. Phys. Chem.* **2000**, *19*, 409-453.

(11) Creighton, J. A.; Eadon, D. G. Ultraviolet-Visible Absorption Spectra of the Colloidal Metallic Elements. *J. Chem. Soc.-Faraday Trans.* **1991**, *87*, 3881-3891.

(12) Jain, P. K.; Huang, X. H.; El-Sayed, I. H.; El-Sayed, M. A. Noble Metals on the Nanoscale: Optical and Photothermal Properties and Some Applications in Imaging, Sensing, Biology, and Medicine. *Accounts Chem. Res.* **2008**, *41*, 1578-1586.

(13) Grzelczak, M.; Perez-Juste, J.; Mulvaney, P.; Liz-Marzan, L. M. Shape control in gold nanoparticle synthesis. *Chem. Soc. Rev.* **2008**, *37*, 1783-1791.

(14) Perez-Juste, J.; Pastoriza-Santos, I.; Liz-Marzan, L. M.; Mulvaney, P.; Elsevier Science Sa: 2005, p 1870-1901.

(15) Kreibig, U.; Vollmer, M. *Optical Properties of Metal Clusters. (Springer Series in Materials Science 25)*, 1995.

(16) Freund, P. L.; Spiro, M. Colloidal catalysis: the effect of sol size and concentration. *J. Phys. Chem.* **1985**, *89*, 1074-1077.

(17) Nikoobakht, B.; El-Sayed, M. A. Preparation and growth mechanism of gold nanorods (NRs) using seed-mediated growth method. *Chem. Mat.* **2003**, *15*, 1957-1962.

(18) Yen, C. W.; Mahmoud, M. A.; El-Sayed, M. A. Photocatalysis in Gold Nanocage Nanoreactors. *J. Phys. Chem. A* **2009**, *113*, 4340-4345.

(19) Sun, Y. G.; Xia, Y. N. Shape-controlled synthesis of gold and silver nanoparticles. *Science* **2002**, *298*, 2176-2179.

(20) Mahmoud, M. A.; El-Sayed, M. A. Comparative study of the assemblies and the resulting plasmon fields of Langmuir-Blodgett assembled monolayers of silver nanocubes and gold nanocages. *J. Phys. Chem. C* **2008**, *112*, 14618-14625.

(21) Anon. *What causes the colors of metals like gold?* 12/15/2010. http://www.webexhibits.org/causesofcolor/9.html.

(22) Jensen, T. R.; Duval, M. L.; Kelly, K. L.; Lazarides, A. A.; Schatz, G. C.; Van Duyne, R. P. Nanosphere lithography: Effect of the external dielectric medium on the surface plasmon resonance spectrum of a periodic array of sliver nanoparticles. *J. Phys. Chem. B* **1999**, *103*, 9846-9853.

(23) Reinhard, B. M.; Siu, M.; Agarwal, H.; Alivisatos, A. P.; Liphardt, J. Calibration of dynamic molecular rule based on plasmon coupling between gold nanoparticles. *Nano Lett.* **2005**, *5*, 2246-2252.

(24) Fromm, D. P.; Sundaramurthy, A.; Schuck, P. J.; Kino, G.; Moerner, W. E. Gap-dependent optical coupling of single "Bowtie" nanoantennas resonant in the visible. *Nano Lett.* **2004**, *4*, 957-961.

(25) Tabor, C.; Murali, R.; Mahmoud, M.; El-Sayed, M. A. On the Use of Plasmonic Nanoparticle Pairs As a Plasmon Ruler: The Dependence of the Near-Field Dipole Plasmon Coupling on Nanoparticle Size and Shape. *J. Phys. Chem. A* **2009**, *113*, 1946-1953.

(26) Hao, E.; Schatz, G. C. Electromagnetic fields around silver nanoparticles and dimers. *J. Chem. Phys.* **2004**, *120*, 357-366.

(27) Huang, W. Y.; Qian, W.; Jain, P. K.; El-Sayed, M. A. The effect of plasmon field on the coherent lattice phonon oscillation in electron-beam fabricated gold nanoparticle pairs. *Nano Lett.* **2007**, *7*, 3227-3234.

(28) Fischer, U. C.; Zingsheim, H. P. Submicroscopic pattern replication with visible light. *J. Vac. Sci. Technol.* **1981**, *19*, 881-885.

(29) Jin, R.; Wu, G.; Li, Z.; Mirkin, C. A.; Schatz, G. C. What controls the melting properties of DNA-linked gold nanoparticle assemblies? *J. Am. Chem. Soc.* **2003**, *125*, 1643-1654.

(30) Haes, A. J.; Chang, L.; Klein, W. L.; Van Duyne, R. P. Detection of a biomarker for Alzheimer's disease from synthetic and clinical samples using a nanoscale optical biosensor. *J. Am. Chem. Soc.* **2005**, *127*, 2264-2271.

(31) Berger, C. E. H.; Beumer, T. A. M.; Kooyman, R. P. H.; Greve, J. Surface plasmon resonance multisensing. *Anal. Chem.* **1998**, *70*, 703-706.

(32) Brigger, I.; Dubernet, C.; Couvreur, P. Nanoparticles in cancer therapy and diagnosis. *Adv Drug Deliv Rev* **2002**, *54*, 631-651.

(33) Aymonier, C.; Schlotterbeck, U.; Antonietti, L.; Zacharias, P.; Thomann, R.; Tiller, J. C.; Mecking, S. Hybrids of silver nanoparticles with amphiphilic hyperbranched macromolecules exhibiting antimicrobial properties. *Chem. Commun. (Cambridge, U. K.)* **2002**, 3018-3019.

(34) El-Sayed, I. H.; Huang, X. H.; El-Sayed, M. A. Surface plasmon resonance scattering and absorption of anti-EGFR antibody conjugated gold nanoparticles in cancer diagnostics: Applications in oral cancer. *Nano Lett.* **2005**, *5*, 829-834.

(35) Loo, C.; Lowery, A.; Halas, N.; West, J.; Drezek, R. Immunotargeted nanoshells for integrated cancer imaging and therapy. *Nano Lett.* **2005**, *5*, 709-711.

(36) Fortina, P.; Kricka, L. J.; Graves, D. J.; Park, J.; Hyslop, T.; Tam, F.; Halas, N.; Surrey, S.; Waldman, S. A. Applications of nanoparticles to diagnostics and therapeutics in colorectal cancer. *Trends Biotechnol.* **2007**, *25*, 145-152.

(37) Neretina, S.; Qian, W.; Dreaden, E. C.; El-Sayed, M. A.; Hughes, R. A.; Preston, J. S.; Mascher, P. Exciton Lifetime Tuning by Changing the Plasmon Field Orientation with Respect to the Exciton Transition Moment Direction: CdTe-Au Core-Shell Nanorods. *Nano Lett.* **2009**, *9*, 1242-1248.

(38) Biesso, A.; Qian, W.; El-Sayed, M. A. Gold nanoparticle plasmonic field effect on the primary step of the other photosynthetic system in nature, bacteriorhodopsin. *J. Am. Chem. Soc.* **2008**, *130*, 3258-+.

CHAPTER 2

Nanoparticle Synthesis and Arrangement

The great interest in “nano” has come from the entirely new set of properties that occur when a material is brought to these small dimensions. There are many methods for nanoparticle production; two distinguish themselves as the most useful. The colloidal method involves the growth of the particle from the bottom-up approach. A metal salt is reduced in solution and simultaneously capped with a surface protecting ligand. The other major approach for nanoparticle production utilizes a top-down approach. Electron-beam lithography and nanosphere lithography utilize vapor deposition of metals over chemical masks. The subsequent removal of the chemical mask results in well-defined nanoparticles. Nanoparticles produced lithographically are created in arrays that are in fixed positions a solid surface. To create arrays of colloidally produced particles, additional deposition methods must be applied. The Langmuir-Blodgett method takes advantage of amphiphilic capping ligands by suspending particles on an air-water interface. These methods and additional characterization techniques are described in this chapter.

2.1 Introduction

2.1.1 Colloidal Growth of Nanoparticles

The very intricate nanoparticle shapes (Figure 2.1) mentioned herein can be created colloidally or through various lithographic procedures. Generally, colloidal methods involve the reduction of a metal salt by a reducing agent, such as sodium citrate or sodium borohydride.[1-3] The complex shapes are derived from surface-passivating ligands that are introduced to the reduction and preferentially bind to a specific facet or facets, slowing their growth.[4-5] This mechanism causes the elimination of fast growing facets, while the other facets become dominant, and can result in geometries such as cubic and rod shaped particles.[6] In many cases, the geometries are well-defined, three-dimensional shapes with a high degree of monodispersity. Additionally, the crystallinity of the nanoparticles can be controlled by the method of reduction. Single crystal nanoparticles are preferred because they do not suffer from dephasing, which occurs at domain interfaces and results in dampening of the SPR. The major hurdle of colloidal production of nanoparticles is that their deposition into layers or arrays is particularly difficult to control. When colloidal nanoparticles are combined with an advantageous deposition procedure, elegant structures can be produced and studied. One of the major alternatives to colloidal synthesis is lithographic particle fabrication which is known for precise control.

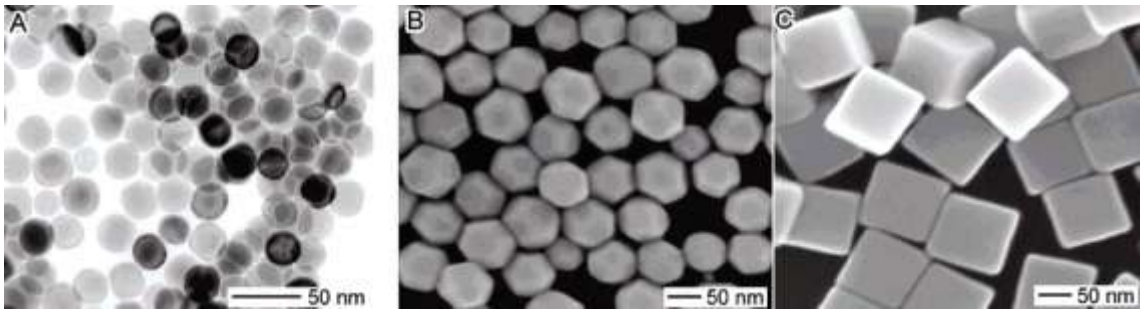

Figure 2.1: SEM images of (A) spheres, (B) truncated cubes, and (C) cubes demonstrating the fine three-dimensional structures that can be produced by the colloidal reduction method.[6]

2.1.2 Lithographic Nanoparticle Fabrication

Lithographic techniques, such as electron-beam and nanosphere lithographies (EBL and NSL, respectfully), rely on vapor deposition of a metal over chemical and particle masks, respectively, to impart the desired two-dimensional particle shape to the condensed metal.[7-8] Once the mask is removed, the particles remain on the solid substrate as an array. These particles have exceptionally well defined shape, monodispersity, and interparticle distance (Figure 2.2). For these reasons, EBL is often used in fundamental studies that are designed to understand the plasmonic field interactions of nanoparticle pairs.[9-10] Although lithography may seem like the answer to the entirety of particle fabrication problems, it does have inherent flaws. NSL is cost-effective and can produce well defined arrays of particles, but particle shape is severely limited by the gaps between adjacent polystyrene-bead masks and the available angle of metal deposition. EBL is capable of "drawing" any shape which can be produced in CAD software, but the technique suffers from high startup and maintenance costs as well as continued cost of maintaining cleanroom facilities. Additionally, lithographically produced particles are amorphous and (although the technology is seemingly "limitless" in two-dimensions)

control over particle shape in the third dimension is limited to changing thickness. Care must be taken to properly assess the requirements of the experiment and resources within a given laboratory setting so that the advantages of a particular particle synthesis method can be utilized.

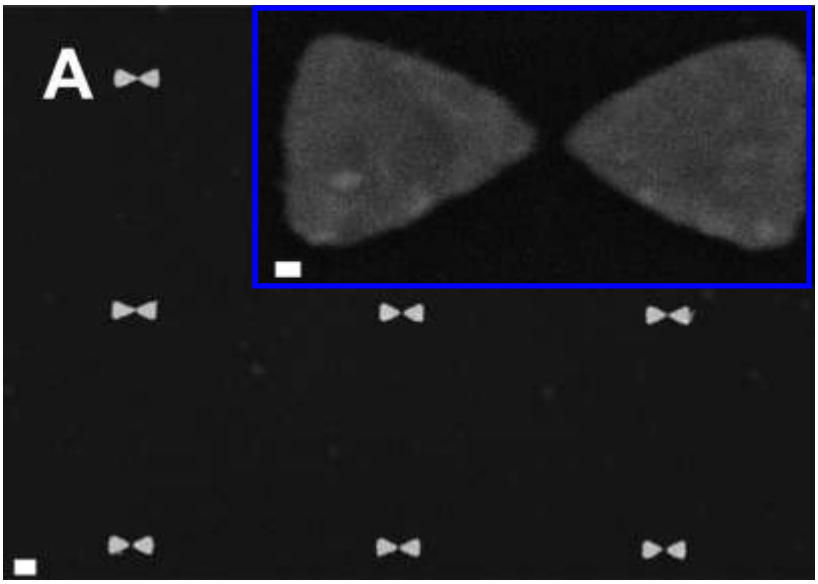

Figure 2.2: SEM image of EBL fabricated gold nanoprisim dimer pairs demonstrating the precise control over array formation and interparticle separation (inset, offset with blue). Dimer pairs are ~14 nm apart at the tips.[10]

2.2 Assembly by Langmuir-Blodgett Deposition

2.2.1 Issues to be Addressed by Langmuir-Blodgett Deposition

Although EBL is the best tool for studying interactions that require precise control, it has its limits. Particles produced by EBL are all two dimensional, amorphous in their structure, and expensive in terms of instrument cost. It would be ideal to exploit a low-cost method of arrangement that can utilize the intricate geometries of colloidally produced particles for similar studies. Conventional deposition methods, such as spin-coating and drop-casting, are insufficient for fundamental studies since they result in

highly disordered multilayers that often display the properties of the bulk material rather than individual nanoparticles, dimers, or trimers of nanoparticles. Self-assembly of nanoparticles onto a surface through binding agents, or simply through electrostatics and/or Van der Walls forces that are already present can yield excellent monolayers, but often results in nearly continuous films.[11] Some control over particle density can be exerted by varying immersion times or surface binding ligand concentration, but this, too, is often "hit or miss" when trying to obtain a series of samples with significantly different average interparticle distances.[11-12] As will be discussed, the Langmuir-Blodgett trough can offer solutions to some of the 2D assembly problems.

2.2.1 Basic Principles of the Langmuir-Blodgett Trough

The Langmuir-Blodgett (LB) technique, which is a traditional method of molecular assembly, has only recently been used for assembly and control of nanoparticle monolayers.[13-15] Figure 2.3 shows the LB trough and its vital components: (A) the dipping mechanism, (B) pressure sensor (Wilhelmy plate and balance), (C) the translating arm, and (D) the trough. The LB technique takes advantage of the ability of amphiphilic molecular or particle species to dissolve in a volatile solvent and then fully and evenly disperse on an immiscible liquid subphase contained in the trough. Upon complete evaporation of the volatile solvent, a floating monolayer of nanoparticles is left behind on the surface of the subphase. Chloroform and water are often used as a solvent/subphase pair due to the low boiling point of chloroform, the high surface tension of water, and the immiscibility of the pair. The translating arm, in contact with the surface of the subphase, is then used to decrease the area available for dispersion of the molecular or particle species. A constant feedback balance measures the surface tension exerted on the

Wilhelmy plate (a paper plate spanning the air-water interface) by the subphase. When a material is placed on the subphase in increasing concentrations, the surface tension is reduced. The change in surface tension from that of the pure subphase is known as the surface pressure.

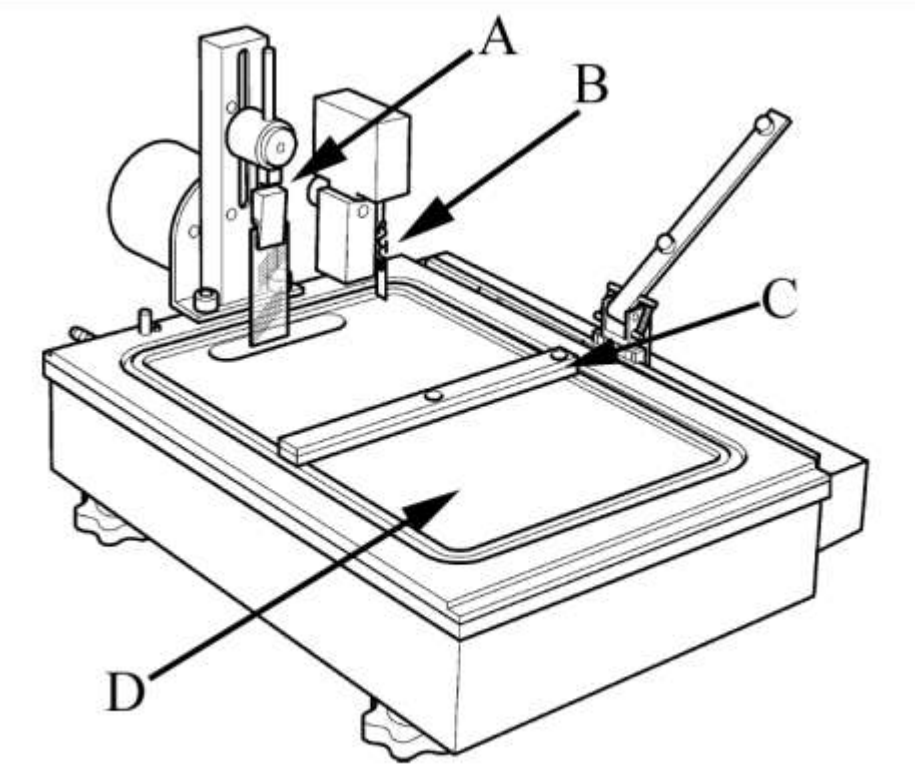

Figure 2.3: Langmuir-Blodgett trough used for nanoparticle, molecular, and polymer deposition. Integral parts: (A) mechanical dipper/sample holder, (B) Wilhelmy plate pressure sensor, (C) translating PTFE arm, and (D) PTFE trough filled with water subphase.[16]

Tao et. al. demonstrated a real-time change in color and optical properties when monolayers of plasmonic silver nanoparticles are compressed on the trough.[17] As the interparticle distance was decreased, the coupling of the nanoparticles could be seen

visually (as a change in color of the floating monolayer) and spectroscopically (as a continual shifting of the extinction band). After compression, the monolayer can be transferred to a substrate by the vertical dipping method at a constant surface pressure. In vertical dipping (Figure 2.4), the substrate is slowly drawn through the monolayer while a constant feedback loop adjusts the surface pressure to compensate for loss of material (from monolayer to substrate) by decreasing the surface area of the trough.

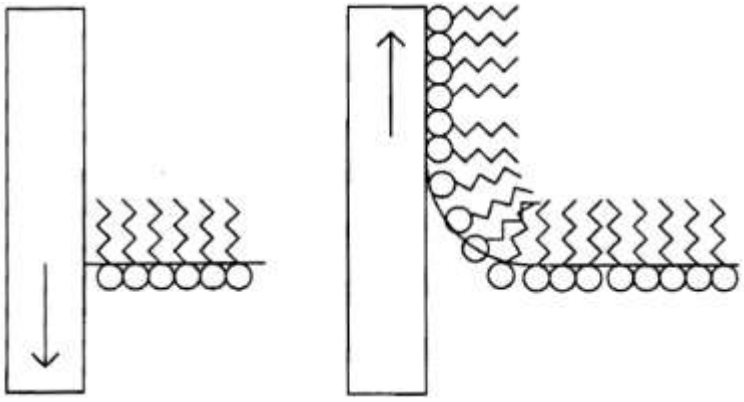

Figure 2.4: Diagram demonstrating the deposition of a molecular monolayer and the behavior of the subphase on the down-stroke (left) and on the upstroke (right).[16]

Monolayers constructed by the LB method contain distributions of nanoparticles centered on a mean interparticle distance. The LB monolayers do not show the same precise control over interparticle separation of particle pairs seen in EBL. It does, however, allow for low-cost application of colloidally prepared nanoparticles to two-dimensional arrays with well-defined average interparticle distances, which is important for practical use. Herein, plasmonic fields, produced by nanoparticle arrays of varied particle coupling, are applied to monolayers of a conjugated fluorescent polymer. The

effect of such intense fields on the emission characteristics of the polymers is discussed in detail.

2.3 Instrumentation and Characterization Techniques

2.3.1 Physical Characterization

A JEOL 100CX TEM was used for initial particle size, shape, and monodispersity analysis of colloidally prepared samples. Array images were taken on a Zeiss Ultra60 SEM to support the size and monodispersity measurements of the TEM and to calculate the percent surface-coverage of the particles on each substrate. An image processing program (ImageJ) was used to determine nanoparticle size, distribution, and surface coverage. Lastly, a Picoscan 5 Molecular Imaging AFM was used for surface profiling of select polymer/nanoparticle assemblies.

2.3.2 Spectroscopic Characterization

Absorbance and steady-state fluorescence measurements were taken on an Ocean Optics HR4000Cg-UV-NIR absorption spectrometer and a Craic 100 microfluorescence spectrometer, respectively. The fluorescence was taken in reflectance mode through a 20x objective lens with 400 nm light excitation from a mercury-arc lamp. Power dependence studies were conducted using neutral density filters to systematically reduce the intensity of the excitation source. For the lifetime measurements, frequency doubled Ti:sapphire laser pulses at 400 nm were used to excite the sample on an inverted microscope, through a 60x water immersion objective. After passing through a monochromator, the emitted photons were detected with an MCP-PMT and recorded using a single photon counting board.

2.4 References

(1) Brust, M.; Walker, M.; Bethell, D.; Schiffrin, D. J.; Whyman, R. Synthesis of Thol-Derivatized Gold Nanoparticles in a 2-Phase Liquid-Liquid System. *J. Chem. Soc.-Chem. Commun.* **1994**, 801-802.

(2) Mallin, M. P.; Murphy, C. J. Solution-phase synthesis of sub-10 nm Au-Ag alloy nanoparticles. *Nano Lett.* **2002**, *2*, 1235-1237.

(3) Link, S.; Wang, Z. L.; El-Sayed, M. A. Alloy formation of gold-silver nanoparticles and the dependence of the plasmon absorption on their composition. *J. Phys. Chem. B* **1999**, *103*, 3529-3533.

(4) Nikoobakht, B.; El-Sayed, M. A. Preparation and growth mechanism of gold nanorods (NRs) using seed-mediated growth method. *Chem. Mat.* **2003**, *15*, 1957-1962.

(5) Sun, Y. G.; Xia, Y. N. Shape-controlled synthesis of gold and silver nanoparticles. *Science* **2002**, *298*, 2176-2179.

(6) Wiley, B.; Sun, Y.; Mayers, B.; Xia, Y. Shape-Controlled Synthesis of Metal Nanostructures: The Case of Silver. *Chemistry- A European Journal* **2005**, *11*, 454-463.

(7) Haynes, C. L.; Van Duyne, R. P. Nanosphere lithography: A versatile nanofabrication tool for studies of size-dependent nanoparticle optics. *J. Phys. Chem. B* **2001**, *105*, 5599-5611.

(8) Xia, Y. N.; Rogers, J. A.; Paul, K. E.; Whitesides, G. M. Unconventional methods for fabricating and patterning nanostructures. *Chem. Rev.* **1999**, *99*, 1823-1848.

(9) Huang, W. Y.; Qian, W.; Jain, P. K.; El-Sayed, M. A. The effect of plasmon field on the coherent lattice phonon oscillation in electron-beam fabricated gold nanoparticle pairs. *Nano Lett.* **2007**, *7*, 3227-3234.

(10) Tabor, C.; Murali, R.; Mahmoud, M.; El-Sayed, M. A. On the Use of Plasmonic Nanoparticle Pairs As a Plasmon Ruler: The Dependence of the Near-Field Dipole Plasmon Coupling on Nanoparticle Size and Shape. *J. Phys. Chem. A* **2009**, *113*, 1946-1953.

(11) Daniel, M. C.; Astruc, D. Gold nanoparticles: Assembly, supramolecular chemistry, quantum-size-related properties, and applications toward biology, catalysis, and nanotechnology. *Chem. Rev.* **2004**, *104*, 293-346.

(12) Liu, S. T.; Zhu, T.; Hu, R. S.; Liu, Z. F. Evaporation-induced self-assembly of gold nanoparticles into a highly organized two-dimensional array. *Phys. Chem. Chem. Phys.* **2002**, *4*, 6059-6062.

(13) Mahmoud, M. A.; El-Sayed, M. A. Aggregation of Gold Nanoframes Reduces, Rather Than Enhances, SERS Efficiency Due to the Trade-Off of the Inter- and Intraparticle Plasmonic Fields. *Nano Lett.* **2009**, *9*, 3025-3031.

(14) Tao, A.; Kim, F.; Hess, C.; Goldberger, J.; He, R. R.; Sun, Y. G.; Xia, Y. N.; Yang, P. D. Langmuir-Blodgett silver nanowire monolayers for molecular sensing using surface-enhanced Raman spectroscopy. *Nano Lett.* **2003**, *3*, 1229-1233.

(15) Huang, J. X.; Kim, F.; Tao, A. R.; Connor, S.; Yang, P. D. Spontaneous formation of nanoparticle stripe patterns through dewetting. *Nat. Mater.* **2005**, *4*, 896-900.

(16) Anon.; Nima Technology.

(17) Tao, A.; Sinsermsuksakul, P.; Yang, P. Tunable plasmonic lattices of silver nanocrystals. *Nat. Nanotechnol.* **2007**, *2*, 435-440.

CHAPTER 3

POLY(P-PHENYLENEETHYNYLENE) FLUORESCENT POLYMER

Abstract

Conjugated polymers have become a new frontier for device fabrications because of their low cost, flexibility, and versatility. The poly(p-phenyleneethynylene) polymers are a class of polymers that have set themselves apart from other materials because of their high fluorescence yield and general sensitivity to external stimuli, which makes them particularly suited for use as sensors. This chapter shall serve to introduce the origins of poly(p-phenyleneethynylene) polymer's unique optical properties by explaining oligomeric properties, geometric restrictions in the ground and excited states, and aggregation and interchain effects on electronic properties.

3.1 General Overview

Conjugated polymers have been studied extensively for their use in electronic devices as well as in sensory applications because of their strong absorption, emission, and conduction properties.[1-3] Specifically, the poly(p-phenyleneethynylene) (PPE) fluorescent polymer has been used to sense transition metal complexes,[4] ethylene gas,[5] and bacteria.[6] The versatiliy of PPE comes from its high quantum yield, the ability to render the polymer water-solubile (while retaining luminescence), and the sensitivity of the polymer to external changes. Part of what makes the PPEs unique is the incorperation of triple bonds into their conjugated structure. Figure 3.1 shows the PPE fluorescent polymer that has been used throughout this thesis. In addition to imparting rigidity to the polymer backbone and improving fluorescence, the triple-bond structure causes interesting and useful spectroscopic properties that will be discussed in the following sections.

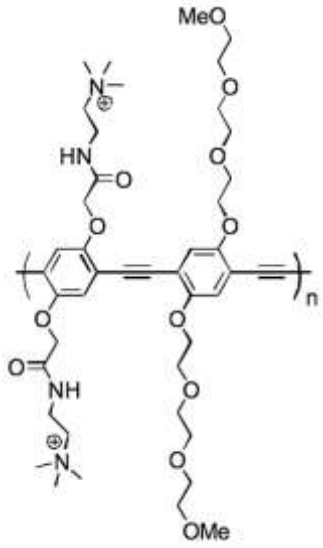

Figure 3.1: Structure of poly(paraphenyleneethynylene) fluorescent polymer used within this thesis of work. The base PPE back bone structure has been functionalized with PEG side-chains and amine terminals to impart hydrophilicity to the polymer

3.2 Origins of PPE Unique Geometric and Photophysical Effects

One of the well-understood aromatic molecules is anthracene (Figure 3.2). Anthracene exhibits ideal spectroscopic behavior (well defined peaks, mirror-symmetry, and a vanishing Stokes shift) due to its ring locked structure, which severely restricts the degrees of freedom within this molecule in the ground and excited states. This type of rigidity, and the spectral effects that accompany it, can be induced in molecules that are not ring-locked like anthracene. Consider two very similar organic structures: the phenyleneethenelene and phenyleneethynelene polymer structures (Figure 3.3 top and bottom, respectively). Both structures exhibit free-rotation around single bonds in the polymer chains and thus have a low torsional barrier in the ground state (GS). In the excited state (ES), aromatic rings adopt the quinoidal structure shown in Figure 3.3. When this occurs in the phenyleneethenelene, the alternating single/double bond character and free rotation are preserved. Alternatively, when the phenyleneethynelene polymer is excited, the presence of triple-bonds causes the generation of a cumulene structure (consecutive double bonds) that severely restricts the possible geometric conformations.[7-8] For this reason, the absorption spectra (GS population) are very broad and the emission spectra (ES population) are very narrow. Typical absorption and emission spectra of the phenyleneethynelene materials exhibit asymmetric peaks with a sharp cusp at once side, owing to the quadratic-type coupling that occurs between the vastly different energy potentials of the GS and ES.

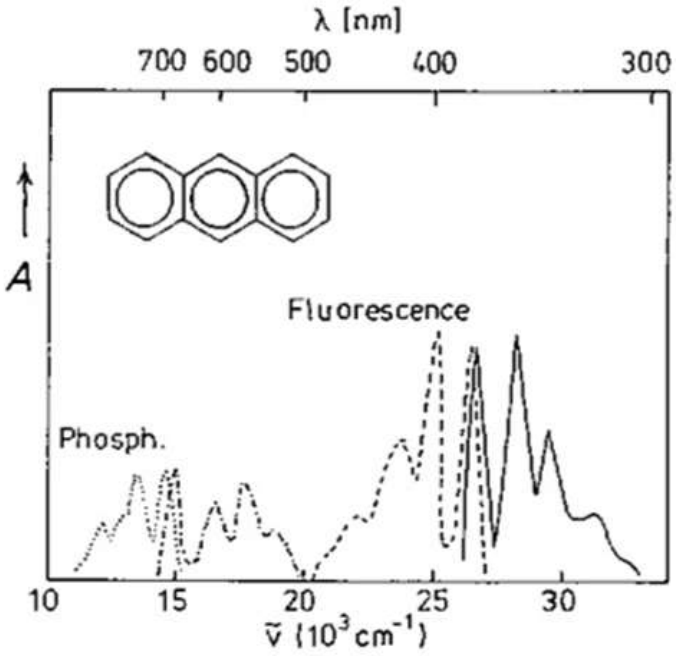

Figure 3.2: Absorption (solid) and emission (dash and dot) from anthracene. Inset shows the fused ring structure of anthracene.[9]

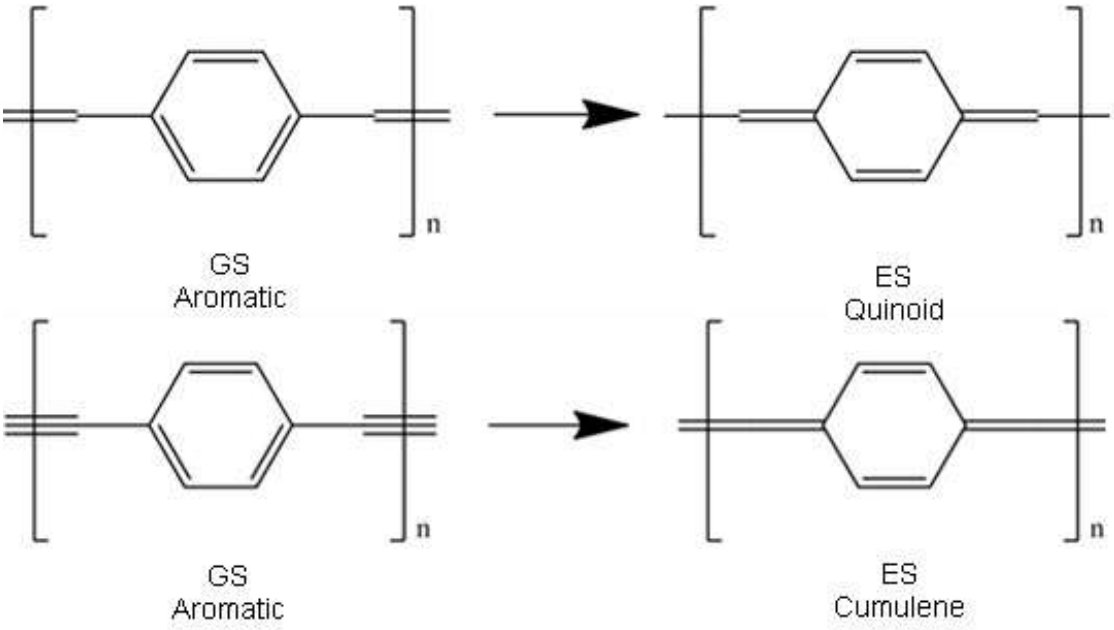

Figure 3.3: GS and ES structures of phenyleneethenelene (top) and phenyleneethynelene polymers. In both molecules the phenyl ring adopts a quinoid structure, but the triple-bonds in the phenyleneethynelene are responsible for generating a consecutive double bond structure known as a cumulene.

3.3 PPE Aggregate and Assembly Effects

The conformational effects on PPE polymer fluorescence have been investigated quite extensively as a function of polymer chain aggregation.[10-13] Planarization of the phenyl rings in the backbone, which is opposed by entropy when chains are isolated, occurs when the polymers aggregate in a poor solvent or in a solid film. Wang et. al. conducted a water titration of a hydrophobic PPE polymer dissolved in DMF. With the addition of water, vastly different spectral properties evolved as isolated species gave way to polymer aggregates, and the emission red-shifted from blue-emitting to yellow emitting species (spectra shown in Figure 3.4 and conceptualized in Figure 3.5). Planarization leads to extended conjugation, which lowers the electronic energy levels slightly and red-shifts emission.[14] In more disordered systems, where the pi systems of the aromatic rings can overlap with each other, a significant decrease in energy is observed with profound red-shifting and characteristic broad emission for pi-pi overlap of ground-state and excimeric species.[15]

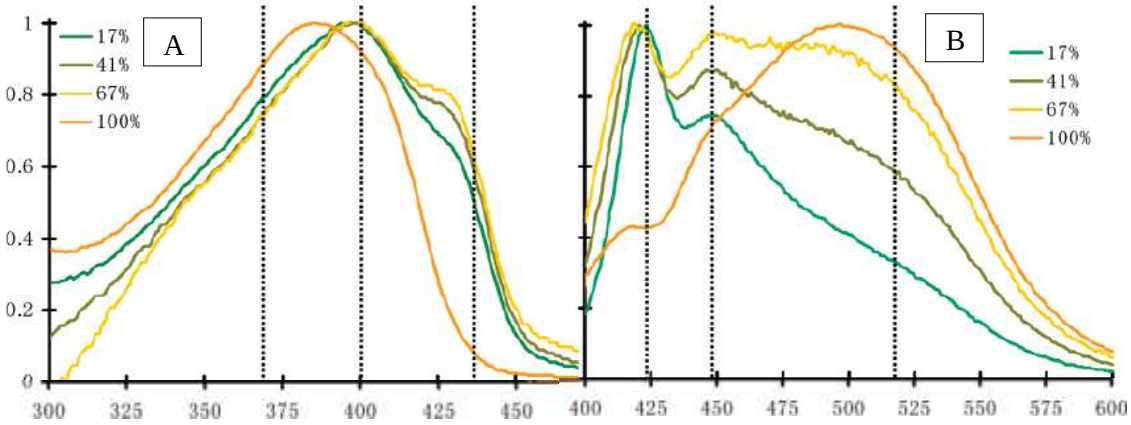

Figure 3.4:Absorption (A) and emission (B) of a hydrophobic PPE fluorescent polymer in solutions containing varied percentages of water in DMF (17-100 % water).The emission becomes exceptionally broad in the case of the 100% water sample, where aggregation is at its highest.[14]

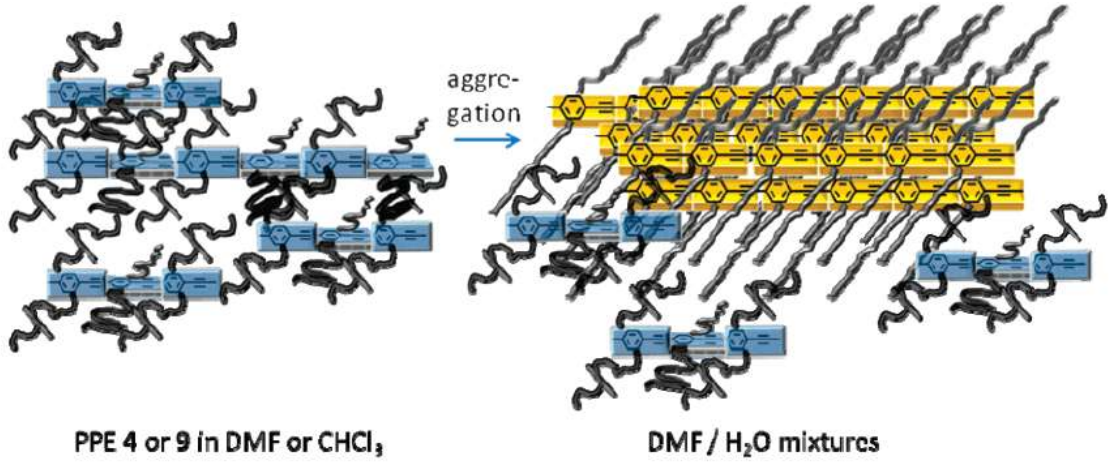

Figure 3.5: Conceptualization of the aggregation and emission characteristics of PPE fluorescent polymer. Blue emitting species are present in the isolated polymer chains, but upon aggregation, planarization, and interchain interactions, emission red-shifts to yellow.[14]

3.4 References

(1)Bunz, U. H. F. Poly(p-phenyleneethynylene)s by alkyne metathesis. *Accounts Chem. Res.* **2001**, *34*, 998-1010.

(2)Feng, F. D.; He, F.; An, L. L.; Wang, S.; Li, Y. H.; Zhu, D. B. Fluorescent conjugated polyelectrolytes for biomacromolecule detection. *Adv. Mater.* **2008**, *20*, 2959-2964.

(3)McQuade, D. T.; Pullen, A. E.; Swager, T. M. Conjugated polymer-based chemical sensors. *Chem. Rev.* **2000**, *100*, 2537-2574.

(4)Wang, H. Y.; Lin, J. M.; Huang, W.; Wei, W. Fluorescence "turn-on" metal ion sensors based on switching of intramolecular charge transfer of donor-acceptor systems. *Sens. Actuator B-Chem.* **2010**, *150*, 798-805.

(5)Esser, B.; Swager, T. M. Detection of Ethylene Gas by Fluorescence Turn-On of a Conjugated Polymer. *Angew. Chem.-Int. Edit.* **2010**, *49*, 8872-8875.

(6)Phillips, R. L.; Kim, I. B.; Carson, B. E.; Tidbeck, B.; Bai, Y.; Lowary, T. L.; Tolbert, L. M.; Bunz, U. H. F. Sugar-Substituted Poly(p-phenyleneethynylene)s: Sensitivity Enhancement toward Lectins and Bacteria. *Macromolecules* **2008**, *41*, 7316-7320.

(7)Liu, L. T.; Yaron, D.; Berg, M. A. Electron-phonon coupling in phenyleneethynylene oligomers: A nonlinear one-dimensional configuration-coordinate model. *J. Phys. Chem. C* **2007**, *111*, 5770-5782.

(8)Kijima, M.; Kinoshita, I.; Shirakawa, H. Syntheses and properties of conjugated polymers with cumulenic bond in the main chain. *Synth. Met.* **1999**, *101*, 145-148.

(9)Lakowicz, J. R. *Principles of Fluorescence Spectroscopy: 2nd Edition*; Springer, 1999.

(10)Kim, J.; Swager, T. M. Control of conformational and interpolymer effects in conjugated polymers. *Nature* **2001**, *411*, 1030-1034.

(11)Deans, R.; Kim, J.; Machacek, M. R.; Swager, T. M. A poly (p-phenyleneethynylene) with a highly emissive aggregated phase. *J. Am. Chem. Soc.* **2000**, *122*, 8565-8566.

(12)Rathgeber, S.; de Toledo, D. B.; Birckner, E.; Hoppe, H.; Egbe, D. A. M. Intercorrelation between Structural Ordering and Emission Properties in Photoconducting Polymers. *Macromolecules* **2010**, *43*, 306-315.

(13)Kim, J. S.; McHugh, S. K.; Swager, T. M. Nanoscale fibrils and grids: Aggregated structures from rigid-rod conjugated polymers. *Macromolecules* **1999**, *32*, 1500-1507.

(14)Wang, Y. Q.; Zappas, A. J.; Wilson, J. N.; Kim, I. B.; Solntsev, K. M.; Tolbert, L. M.; Bunz, U. H. F. Optical spectroscopy of grafted poly (p-phenyleneethynylene)s in water and Water-DMF mixtures. *Macromolecules* **2008**, *41*, 1112-1117.

(15)Bunz, U. H. F.; Imhof, J. M.; Bly, R. K.; Bangcuyo, C. G.; Rozanski, L.; Bout, D. A. V. Photophysics of poly [p-(2,5-didodecylphenylene)ethynylene] in thin films. *Macromolecules* **2005**, *38*, 5892-5896.

CHAPTER 4

PLASMONIC FIELD ENHANCEMENT OF THE EXCITON-EXCITON ANNIHILATION PROCESS IN A POLY(PARAPHENYLENEETHYNYLENE) FLUORESCENT POLYMER BY SILVER NANOCUBES

Abstract

The poly(paraphenyleneethynylene) fluorescent polymer was assembled alone and on the surface of silver nanocube monolayers using the Langmuir-Blodgett technique. The fluorescence intensity of the polymer was studied as a function of (1) the surface density of pure polymer samples deposited onto quartz substrates, and (2) on the surface coverage of an underlying AgNC monolayer. The pure polymer system demonstrated a continual increase in fluorescence intensity as its surface density increased. However, the fluorescence intensity of the polymer when deposited on the AgNC monolayer initially increased, until a threshold pressure was reached and emission subsequently decreased very rapidly. A power dependence study revealed that one-photon processes were responsible for the initial increased intensity and a two-photon process was occurring after the rapid decrease in the polymer fluorescence. These observations are explained by increases in particle coupling, at increased surface pressure, which enhanced the polymer absorption rate. This first leads to increased emission, followed by a competing process called exciton-exciton annihilation. Even at the relatively low cw-lamp intensities used herein, the large surface plasmon enhancements of the exciting light intensity were able to initiate this high-energy process.

4.1 Introduction

In the solid phase, there is an increased probability of interaction between chains at short distances, which results in an increased number of diffusion pathways of the exciton. Within the polymer matrix, the increased mobility of the excitons leads to a greater likelihood of exciton-exciton interaction. A possible result of this interaction is an annihilation process in which one exciton is excited to a higher excited state at the expense of the other, which is then deactivated non-radiatively to the ground state. This annihilation process has been observed often in polymers, using high rates of excitation from pulsed lasers.[1-4]

For the work in this chapter, we used a relatively weak CW (continuous-wave) excitation source to excite the PPE fluorescent polymer deposited by the LB method over a monolayer of silver nanocubes (AgNCs) of different surface densities. The degree of nanoparticle coupling and, thus, the surface plasmon field strength, was controlled by varying the surface density of the particles during deposition. By creating monolayers, the LB method of arrangement serves to limit the three-dimensional layer-to-layer interaction between the PPE fluorescent polymers that is observed in the literature.[5-6] This yields a less complicated architecture compared to casting methods.

The results contained herein are discussed in terms of the changes in the surface plasmon field strength of the assembled AgNCs, which was shown to enhance the polymer's rate of absorption and is attributed to substantial spectral overlap of the polymer and nanoparticles. Initially, this enhancement leads to an increase in the fluorescence intensity. Then, as the field strength becomes large, the exciton density increases to a level where its collision rate, and thus the bi-exciton non-radiative

annihilation processes, exceeds the polymer fluorescence rate. At this point, the observed polymer fluorescence intensity decrease rapidly.

4.2 Experimental

4.2.1 Reagents and Solvents

ACS reagent grade silver nitrate, polyvinyl pyrolidone (PVP, MW = 55,000), anhydrous ethylene glycol (EG), and spectrophotometeric grade chloroform were obtained from Sigma Aldrich (St. Louis, MO). $AgNO_3$ solutions were made 15 minutes prior to addition to avoid oxidation by EG. Reagent grade sodium sulfide nona-hydrate was purchased from MP Biomedicals (Solon, OH). The 3 mM sodium sulfide solution was made through serial dilution of a 30 mM stock solution. Reagent grade methanol and acetone were purchased from BDH Middle East (Dubai, UAE).

4.2.2 Silver Nanocube synthesis

The AgNCs were prepared by heating 30 mL of EG at 150^{o}C for 1 hour with constant stirring.[7-9] EG was the solvent for all subsequent solutions in this synthesis. The heating of EG was followed by the addition of a solution of PVP (10 mL, 2.52×10^{-1}M by repeat unit). Before continuing, the temperature of the resultant solution was allowed to stabilize back to 150^{o}C. Next, sodium sulfide (0.4 mL, 3×10^{-3}M), was added and followed subsequently by the slow injection of $AgNO_3$ (3.6 mL, 2.82×10^{-1}M) into the reaction mixture. The silver ions were reduced completely after 15 minutes, producing AgNCs. For the purification of the particles, 5 mL of the AgNC solution was diluted with acetone, centrifuged, and then redispersed in water. Shortly before LB dispersion of the particles into a monolayer, the particles were centrifuged once more and dispersed in 10 mL of chloroform. Lastly, AgNCs were passed through a 0.2 µm PTFE syringe filter.

Nanoparticles were analyzed by TEM and determined to have a particle size of 58 ± 6 nm. The histogram of particle size distribution is show in Figure A.1.

4.2.3 PPE Polymer Preparation

The poly(paraphenyleneethynylene) fluorescent polymer was made by Ronnie Phillips in the laboratory of Uwe Bunz. The synthesis of the PPE fluorescent polymer is discussed in detail within Appendix A. Briefly, the PPE fluorescent polymer synthesis began with the preparation of the fundamental building blocks as shown in Figure A.4. Palladium catalyzed coupling of monomers 1 and 2 furnished PPE 3, which was reacted with unsym-dimethylethylene-diamine to furnish PPE 4. Upon reaction with iodomethane, PPE 5 resulted as an orange powder. According to gel permeation chromatography (GPC) vs. polystyrene, PPE 5 has a molecular weight (M_n) and polydispersity index (PDI) of 1.1 x 10^4 and 1.95, respectively. Shortly before dispersion, the PPE 5 polymer was dissolved in a few drops of methanol as a bridging solvent into chloroform. From here on, PPE 5 will simply be referred to as PPE.

4.2.4 Langmuir-Blodgett Deposition of AgNCs and PPE Fluorescent Polymer

The AgNCs were assembled with the use of a Nima 611 D trough. Before nanoparticle dispersion, the surface of the water subphase was cleaned by closing the translating arm of the LB trough and removing suspended contaminants with a small pump equipped with a PTFE tip. A subsequent pressure-area isotherm was completed to verify a pristine water surface. To begin, 50 µL aliquots of AgNCs in chloroform were sprayed over the surface of the water-filled trough. Time was allowed for the chloroform to fully evaporate, leaving the particles uniformly dispersed on the subphase. The surface

pressure was monitored with the use of a Wilhelmy plate, attached to a D1L-75 model pressure sensor. The mechanical barrier was then closed to achieve increased surface pressures. These pressures were adjusted between samples to attain variation in the percent surface coverage of nanoparticles. A motorized dipper was used to deposit the AgNCs on a quartz or silicon substrate by drawing it through the floating monolayer.

Using the same deposition procedure mentioned above, a layer of the PPE fluorescent polymer was dispersed, compressed, and deposited onto the previously made nanoparticle arrays (or alone onto a bare substrate) at constant surface pressures. All polymer and AgNC films were each deposited from the same monolayer to ensure uniform assembly.

4.3 Results and Discussion

4.3.1 Imaging of the AgNC monolayer before and after deposition of the PPE polymer

AgNCs were assembled on both quartz and silicon substrates at surface pressures of 6, 5, 4, 3, 1, 0.5, and 0 mN/m. Figure 4.1 shows the SEM images of four of these samples, which were assembled at surface pressures of 0, 1, 4, and 6 mN/m, A-D respectively. The SEM images for 0.5, 3, and 5 mN/m samples are shown in Figure A.2. The SEM images were used to characterize the morphology of the silver nanoparticle samples assembled on the surface of silicon substrates. From the SEM images, the size-distribution was determined to be monodisperse with an average edge length of 58 nm (SD = 6 nm). The surface coverage (which determines the monolayer surface density and interparticle distance) changed as a function of the surface pressure at which the particles were deposited onto the substrate. SEM imaging also allowed for the calculation of the percent of surface coverage and the average interparticle distance. The surface coverage

was found to be 5.7, 6.5, 9.0, 10.1, 10.7, 11.2, and 13.8% for the samples assembled at pressures of 0, 0.5, 1, 3, 4, 5, and 6 mN/m, respectively.

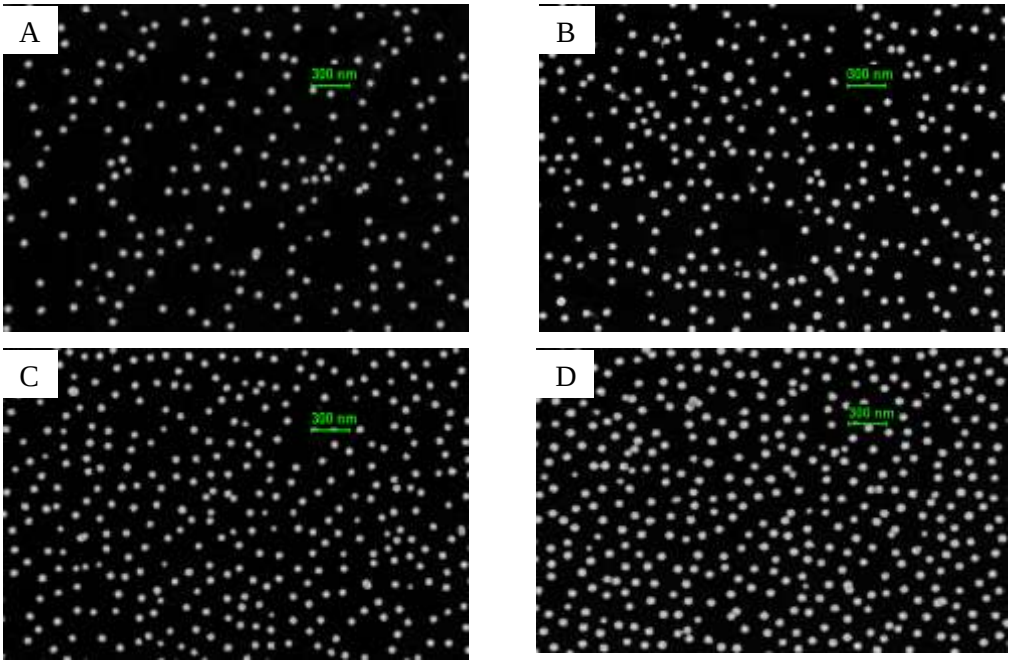

Figure 4.1 (A-D) SEM images of PVP capped AgNC monolayers that have been assembled on silicon substrates at surface coverage of 5.7, 9.0, 10.7, and 13.8%, respectively. A monodisperse population of AgNCs was observed with an average particle diameter of 58 nm (SD = 6 nm).

Although SEM imaging provided a good idea of the morphology of the monolayer in two-dimensions, it lacked any 3D information. Atomic force microscopy (AFM) was used to gain insight into the monolayer topography. Contrary to SEM, AFM images contain details relating to both the polymer and the AgNCs. Figure 4.2 shows the AFM images of AgNC monolayers that were coated with PPE polymer after being assembled to surface coverage of 13.8% (Figure 4.2: A & C) and 5.7% (Figure 4.2: B & D). The 2D image view of AgNC monolayers corresponds well with the SEM images in terms of particle arrangement. This means that the monolayer did not change

significantly during the deposition of the PPE polymer layer. The thickness of the polymer layer was calculated from the z-component of the AFM topographic images shown in Figure 4.2B and 4.2C. According to the SEM images, the edge length of the AgNC is 58 ± 6 nm. The height of the AgNC-polymer structures, in Figure 4.2C and 4.2D, is determined to be 65 nm. This yields a polymer thickness of ~7 nm. The standard deviation (SD) in the particle dimensions, from the SEM, overlaps slightly w/ the SD of the dimensions of the AgNC/PPE (the difference being 7 ± 8 nm for the thickness of the polymer layer). Although we cannot ascertain an exact polymer thickness from these measurements, we are certain the shift in average particle diameter between the SEM and AFM arises from the addition of PPE polymer and has a value in the above mentioned range.

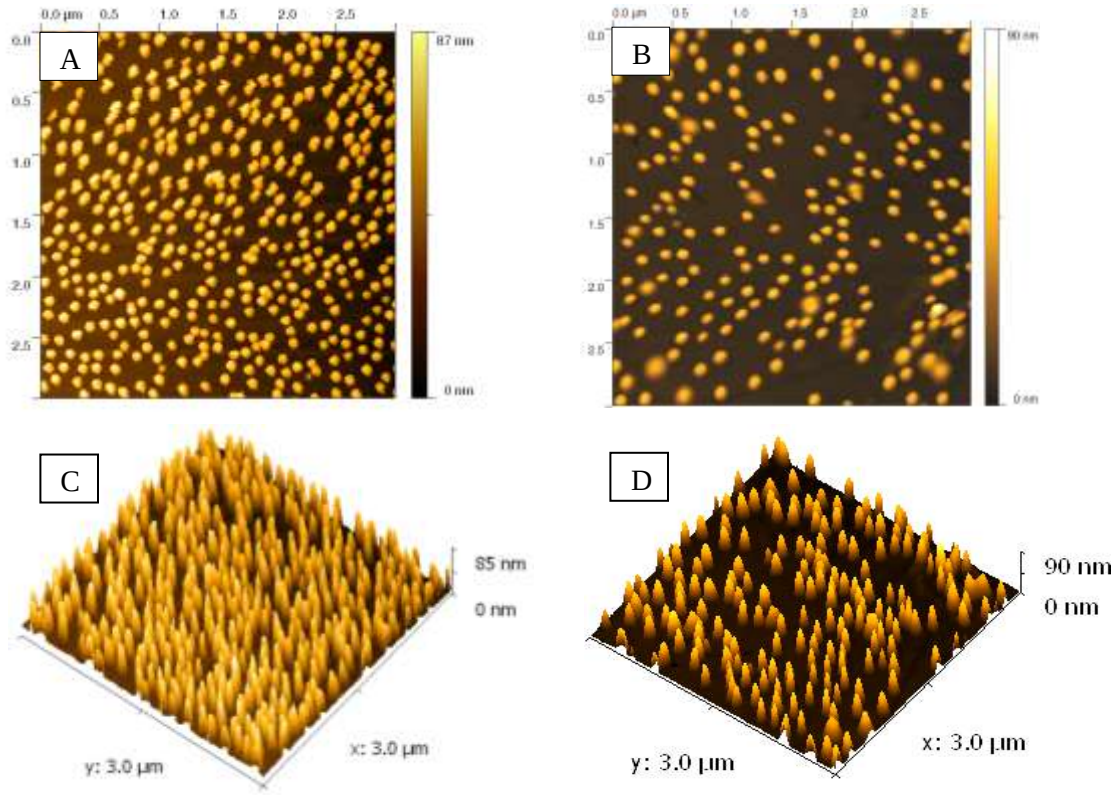

Figure 4.2 AFM 2D and 3D representations of monolayers of PVP capped AgNCs that have been deposited on quartz substrates and covered with a thin layer of PPE polymer. AgNCs were assembled to surface coverage of 13.8% (A & C) and 5.7% (B & D). AFM measurements give a particle-plus-polymer diameter of 65 nm. Combining AFM and SEM measurements, the thickness of the PPE polymer that was deposited onto the nanoparticle monolayer was determined to be ~7 nm.

4.3.2 Statistical analysis of the interparticle distance as a function of surface pressure

The average center-to-center interparticle distance was determined from nearest neighbor particle measurements within the SPIP image processing software and found to range from 157 to 130 nm (5.7 % to 13.8 % coverage). The center-to-center interparticle distance was the mean value taken from the distribution of particle pairs. These distributions are displayed in Figure 4.3 as a series of histograms that show a shifting of the particle pair population to smaller interparticle separations. More significant than the separation, the distributions show a narrowing of the population (described by the values

of the standard deviation) and a continued increase in the number of particle pairs from low surface coverage to higher coverage.

An interesting progression of the particle distributions, which is characteristic of LB monolayers, can be seen in Figure 4.3. The low-surface-coverage sample (A) shows a broad distribution of randomly oriented particles. This is referred to as the "gas phase" when assembling monolayers on the LB trough.[10] The samples ranging from 9.0% to 10.7% coverage (B-D) show a narrowed population, and the distribution is tending toward a lower interparticle separation. This increased region of compression is known as the "liquid phase," because the particles are adopting a condensed arrangement with greater order. Lastly, the highest-surface-coverage samples (E and F) can be related to the "solid phase" because of the noticeably narrower distribution and increased concentration of particles. The combined effect of proximity and particle density leads to a great extent of multi-particle coupling, which is responsible for the observed large enhancements of particle near-fields. The decrease of the interparticle separation occurs as the particles are spatially influenced by an increasing number of neighbors that are forced into the same area (at higher surface pressures) during the assembly on the LB trough. This increased pressure leads to a narrowing of the distribution due to the restricted movement of the particles. Overall there are many more particles interacting at close interparticle distances and with narrower ranges when the surface pressure is continually increased.

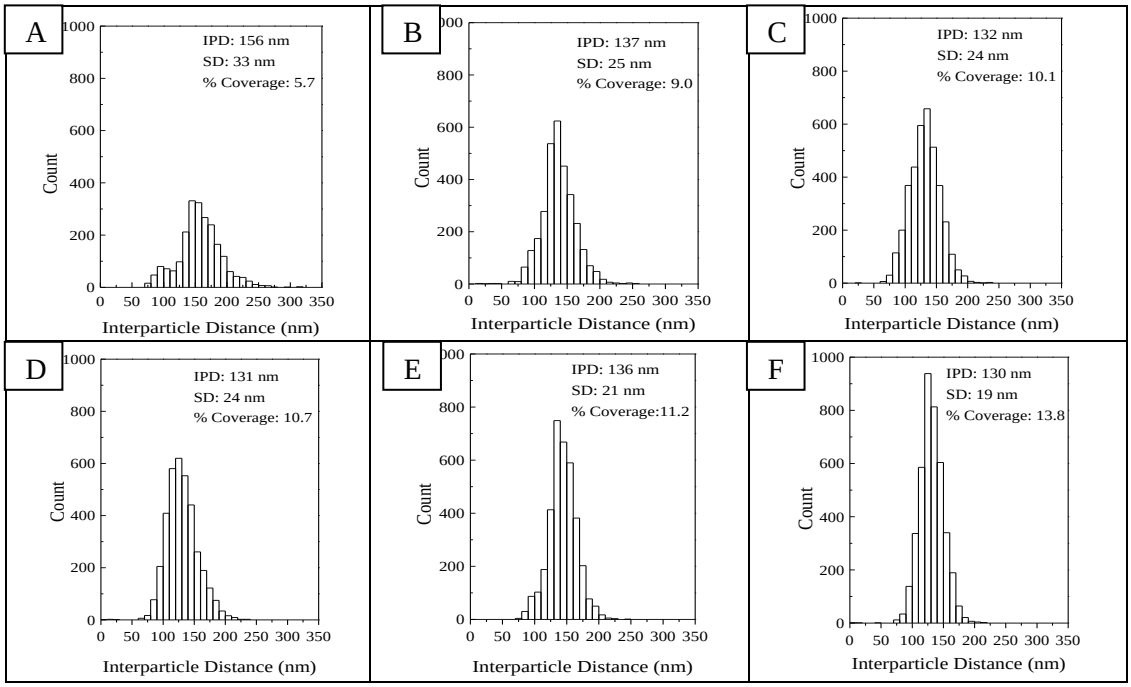

Figure 4.3: Distribution of nearest neighbor AgNC interparticle distances within each sample, assembled on the LB trough at different surface coverage: (A) 5.7%, (B) 9.0%, (C) 10.1%, (D) 10.7%, (E) 11.2%, and 13.8%. The distribution of particles narrows, shifts to lower interparticle distance, and the number of particle pairs increases as the percent coverage is increased. The 6.5% coverage is not shown due to its similarity to the 5.7% coverage sample, with the exception of yielding a higher number of particles pairs.

4.3.2 Plasmon spectra of AgNCs and AgNCs coated with PPE polymer

Silver nanocubes have three surface plasmon spectral peaks.[7] Figure 4.4A shows the surface plasmon resonances of 58 nm PVP capped AgNCs deposited into monolayers at surface coverage of 5.7, 6.5, 9.0, 10.1, 10.7, 11.2, and 13.8%. The dipolar coupling of neighboring AgNC particles lead to a decrease in the plasmon oscillation frequency and gives the observed red-shift with increasing surface coverage (Figure 4.4A).[10] The spectra of AgNC monolayers coated with PPE polymer are shown in Figure 4.4B. The SPR spectral peak positions red-shift as the interparticle separation decreases (due to plasmonic coupling), but the absorption spectrum of the PPE polymer still strongly overlaps with the primary plasmon peak of the AgNCs. Additionally, a uniform red-shift

of 5-7 nm was observed for the lowest energy peak upon deposition of the PPE polymer onto the AgNC arrays. This shift was due to the change in the local dielectric environment of the particles as the polymer was deposited onto its surface.

To confirm that the polymer is randomly oriented on the AgNC monolayers, polarized fluorescence measurements were conducted. This experiment showed no change in the fluorescence peak intensity or shape with polarized emission. Additionally, SERS measurements showed no observable deviation in the Raman peak positions or intensity as a function of changing excitation polarization. The results of the polarized fluorescence and SERS experiments suggest that the polymer has no preferred molecular orientation or arrangement on the AgNC monolayer; it is therefore assumed to be randomly oriented.

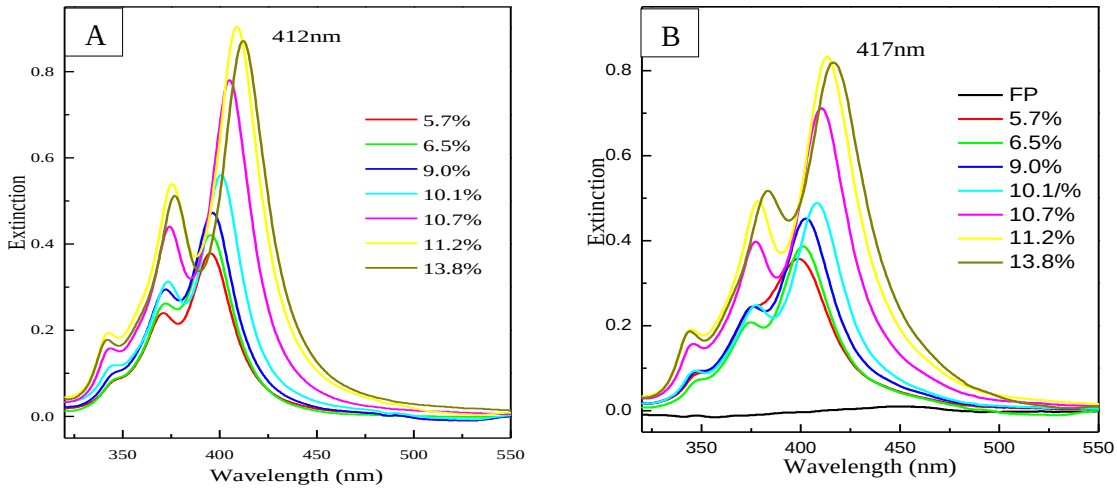

Figure 4.4 UV-visible plasmonic extinction spectra of PVP capped AgNC monolayers that have been deposited on quartz substrates at varied surface coverage before (A) and after (B) coating with a monolayer of PPE polymer. Before polymer coating, a progressive red-shift is observed as the interparticle coupling increased. After deposition of the polymer, a uniform 5-7 nm red-shift is observed in each spectrum due to the change in the local dielectric environment of the particle.

4.3.3 Steady-state fluorescence of pure PPE polymer deposited on AgNC monolayers as a function of Langmuir Blodgett surface pressure

Figure 4.5A shows the absorption spectra of the PPE films deposited onto quartz substrates at different surface pressures. As the surface pressure increased, the degree of compression and, as a result, the amount of polymer in the spectrometer monitoring beam cross-section increased as is indicated by the absorbance increase at 436 nm (Figure 4.5A). Figure 4.5B shows the steady-state fluorescence of the PPE polymer films excited at 400 nm. The fluorescence intensity also increased as the absorption peak intensity increased. The increased number density of the molecules compressed into the beam is reflected as increased absorption and fluorescence intensities.

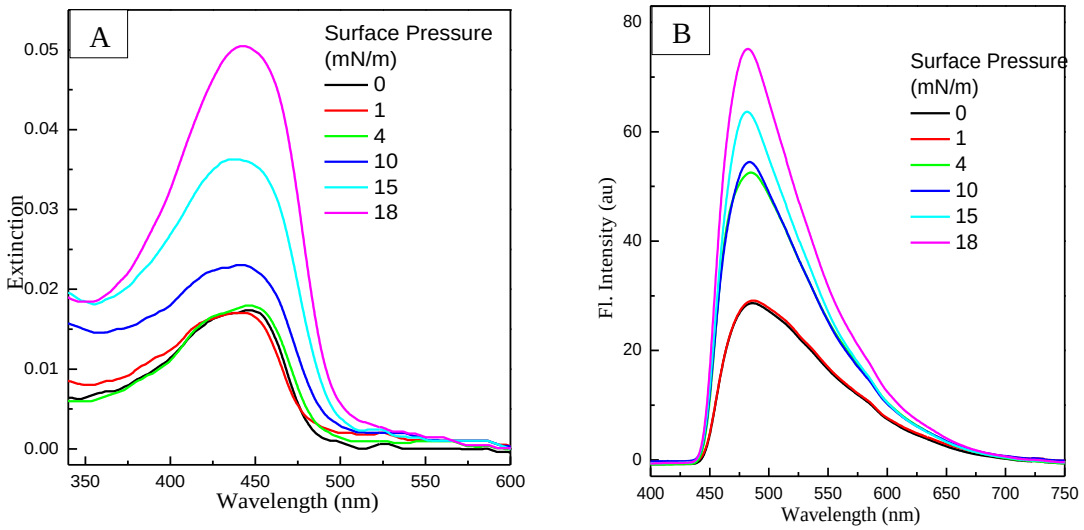

Figure 4.5 (A) UV-visible absorption spectra of PPE polymer films deposited by the LB-trough onto quartz substrates at surface pressures of 0, 1, 4, 10, 15, and 18 mN/m. (B) The corresponding steady-state fluorescence; λ_{ex}= 400 nm. In the case of the pure polymer, the extinction and fluorescence intensities both increased as the surface pressure increased.

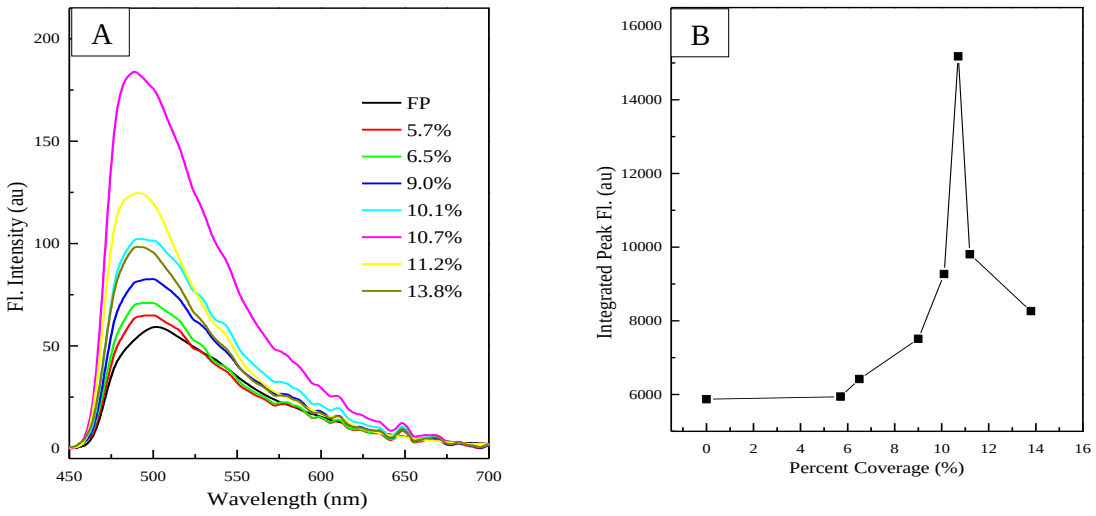

Figure 4.6 (A) Steady-state fluorescence spectra of PPE fluorescent polymer covering PVP capped AgNC monolayers that have been deposited onto quartz substrates to different surface coverage. (B) The relationship between the integrated peak intensity and the surface coverage by AgNCs illustrates the dramatic decrease in the fluorescence intensity that is observed at a surface coverage of 11.2% and beyond.

The steady-state fluorescence of the AgNC-PPE samples that were assembled at different surface coverage is shown in Figure 4.6A, and its trend is shown graphically in Figure 4.6B. The integrated fluorescence band intensity increases with increasing coverage to a maximum value at 10.7% surface coverage followed by a sharp decrease. The fluorescence intensity prior to the rapid decrease shows a fluorescence enhancement of 260% over that of the pure polymer. Both the intensity increase prior to the 10.7% coverage and the quenching phenomenon observed thereafter are proposed to result from the increase in the surface plasmon fields of the AgNC monolayer that is caused by increasing the nanoparticle density. In these experiments, the plasmonic particles have inhomogeneous distributions of interparticle separation distances. Once the interparticle distance reaches a range that enhances the electromagnetic field of the exciting light, surface plasmon enhanced polymer excitation occurs and the fluorescence is enhanced.

Additional increases in the field enhancement result in an increase in the exciton densities that initiate exciton annihilation. When this occurs, the fluorescence intensity decreases, as the rate of annihilation exceeds the rate of enhanced fluorescence. The rapid decrease due to annihilation is proportional to $I^2C^2\sigma$, where I is the lamp intensity, C is the plasmonic enhancement factor, and σ is the fraction area of the excited spot that contains nanoparticles of equal or smaller separation than the critical distance. The plasmonic enhancement factor is very sensitive to the interparticle separation. At or below this critical distance, surface plasmon fields are large enough to allow the rate of annihilation to compete with the rate of fluorescence. Because the distribution of the nanoparticle separation is inhomogeneous in the monolayer (see statistical analysis of interparticle distances shown in Figure 4.3), there is a fraction of particles that are below the critical distance as well as particles that are separated by larger distances. As the surface pressure is increased, the value of σ increases due to the increasing number of particles at the critical distance where the surface fields are strong enough to significantly increase the rate of polymer absorption. This increases exciton densities, resulting in a rate of annihilation that is larger than the rate of fluorescence. It is this increase in the percentage of the overall surface-involvement in annihilation that decreases the observed fluorescence intensity. At high enough surface pressures, all the neighboring particles have distances equal to or shorter than the critical distance, and saturation of fluorescence signal could be observed.

4.3.4 Steady-state fluorescence enhancement of PPE polymer monolayers at different separations from the AgNC monolayer

In order to further support that our observations result from changing the plasmonic field-effect and eliminate a possible mechanism involving either the effect of

the metallic nanoparticles on the polymer configuration or charge transfer processes from the polymer to silver nanoparticles, we carried out an experiment in which the silver monolayers were separated from the fluorescent polymer by different distances. This was accomplished by depositing monolayers of the neutral polymer PVP with different molecular weights (360k and 10k) over the surface of the AgNCs before the PPE was deposited. The integrated fluorescence band intensities of PPE polymer are shown in Figure 4.7 for (A) 360k and (B) 10k PVP spacer layers as the surface pressure of the AgNC monolayer is varied. In both cases, the fluorescence increased initially and then decreased with increasing surface pressure. This, along with the other fluorescence data presented in this paper, seems to suggest that the observed fluorescence intensity increase and subsequent decrease occur regardless of modifications made to the separation between AgNC and PPE polymer layers. From our knowledge that plasmonic fields increase the radiative properties of nearby electronic systems,[11] one can presume that the rate of the polymer absorption increases and leads to an initial enhancement of fluorescence. Further increases in polymer absorption lead to enhanced rates of exciton collision and increased annihilation rates, which decrease the fluorescence intensity. For both spacer layer thicknesses shown in Figure 4.7, the fluorescence intensity follows the pattern just described. At the larger separation distance from the AgNC plasmonic layer provided by the 360k PVP, the fluorescence intensity decrease occurs after a maximum fluorescence of ~30,000 a.u. was reached. When the smaller molecular weight PVP (10k) was used to separate the AgNC monolayer from the PPE polymer layer by a smaller distance, a maximum fluorescence intensity of only ~23,000 a.u. was reached. Thus, at smaller distances from the plasmonic field, the annihilation sets in earlier and does not

allow the enhanced fluorescence to continue to increase to the same extent that was observed with the 360k spacer. This also supports the proposal that the plasmonic field leads absorption enhancement and subsequent annihilation.

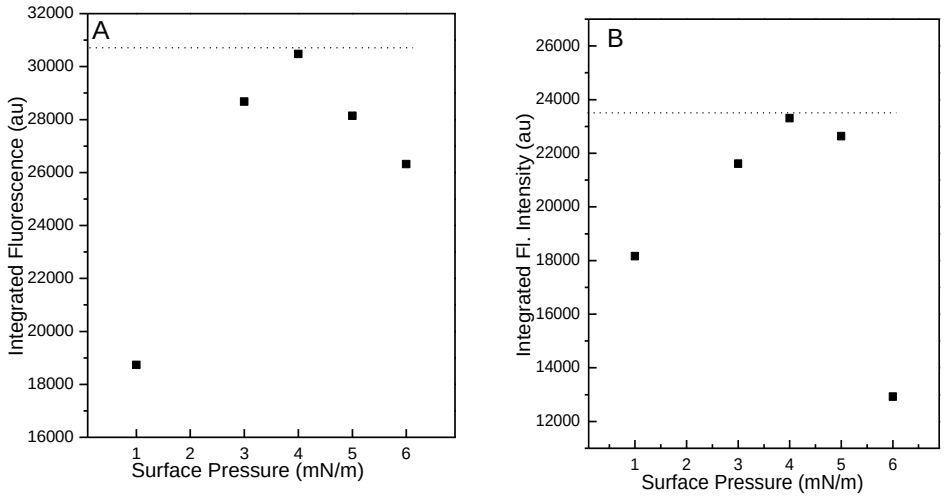

Figure 4.7: Integrated band intensities calculated from the fluorescence spectra of PPE polymer monolayers that were separated from the AgNC monolayer with spacer layers of PVP that have molecular weights of (A) 360,000 and (B) 10,000. In both cases, the fluorescence intensity first increases at low surface pressure, where a turning point occurs and the fluorescence intensity begins to drop at the higher surface pressures. Annihilation sets in earlier at smaller distances from the plasmonic field, limiting the maximum of the fluorescence intensity to a lower value (23,000 au) compared to larger separation distances (30,000 au).

4.3.5 Fluorescence lifetime of pure PPE polymer and PPE polymer deposited on AgNC monolayers

The steady-state fluorescence emission intensity of the PPE polymer is affected by the plasmon field effects of AgNC particle monolayers of varying surface coverage. Figure 4.8A shows the fluorescence decays of the PPE polymer films that were assembled at different surface coverage. The decays were all biexponential, which is typical of concentrated samples of PPE derivatives.[5] Figure 4.8B summarizes the long (top) and the short (bottom) components of the deconvoluted fluorescence decays. The

fluorescence lifetimes of the pure polymer sample (1.19/0.39 ns) were longer than any of the AgNC-PPE samples, while the shortest lifetime was observed from the 10.7% surface coverage sample (0.89/0.28 ns).

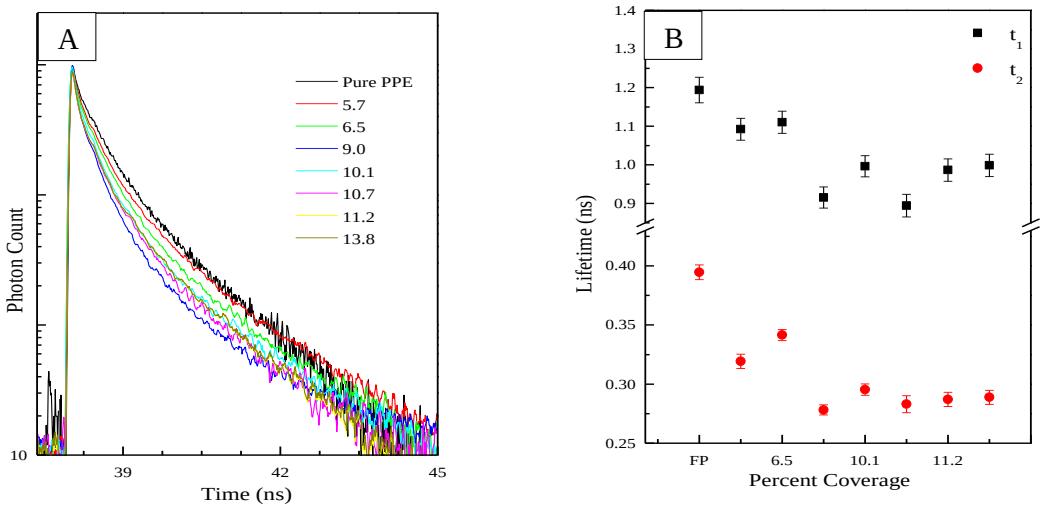

Figure 4.8 (A) Fluorescence intensity decay measurements of pure PPE polymer (black) and PPE polymer on the surface of PVP capped AgNC monolayers that have been deposited onto quartz substrates at different surface coverage. (B) The dependence of the long (top) and the short (bottom) decay components of the deconvoluted fluorescence decay of the polymer as a function of surface coverage of the AgNCs on which the polymer was deposited.

The small changes in the observed lifetimes do not correspond to the large observed decrease in the steady-state fluorescence intensity. The observed drop in intensity that was observed at 11.2% coverage was not accompanied by any change in the corresponding lifetimes. This can be explained by considering how the lifetime experiment is conducted and how steady-state measurements are carried out. When the fluorescent polymer is excited by a pulsed laser in the lifetime experiment, the plasmonic field is only present during the initial excitation pulse width, as it decays very rapidly.

Thus, the observed decay takes place in the absence of any plasmonic excitation of the nanoparticle. Therefore, it is not surprising that the lifetimes are not greatly affected.

4.3.6 Excitation power dependence of the fluorescence intensity

In standard experiments involving exciton-exciton annihilation, an intense pulsed laser is used to vary the pulse intensity over a large range of energy densities. At higher energy densities, the fluorophore generates large quantities of excitons, which can ultimately come into close contact to annihilate each other and reduce the amount of the observed fluorescence per unit energy of the pulse.[1] Exciton-exciton annihilation has been observed previously in thin films of fluorophores.[1,3,12-13] Keplar observed this annihilation process in PPV thin films excited with high-fluence pulsed lasers and observed a decrease of up to 70 % of the original fluorescence yield.

Figure 4.9A shows how the intensity of the PPE polymer fluorescence, in the absence of AgNCs, changed with the exciting light intensity for PPE monolayers deposited at surface pressures of 4 and 15 mN/m. The linear dependence was expected for both samples, as singlet-singlet annihilation does not typically take place in the pure polymer sample at the cw-lamp intensities used. However, when the PPE polymer deposited on top of the nanocubes was excited, a different phenomenon was observed. At low surface coverage of nanocubes, the excitation dependence was linear with a slope of 0.66. At high silver nanocube surface coverage, however, the slope of the linear trend was 1.33, i.e., nearly double the slope that was observed for the low-coverage sample. The drastic difference in the slope values for the two samples suggests that a multi-photon process was occurring on the surface of the excited nanocubes. The reason that

the slopes of the 10.7 and 10.1% AgNC-polymer samples were smaller than the polymer alone (Figure 4.9A) is the result of the surface plasmon field-enhancement of the rate of polymer absorption. Due to enhancement of the Hg-light used, the "apparent" excitation intensity is lower than the actual excitation experienced by the polymer.

In order to demonstrate this enhancement of absorption efficiency in the polymer, the scale on the x-axis (Figure 4.9A, top) was multiplied by a scalar value of 1.51 to reflect the amount of light necessary to elicit the same amount of fluorescence without the presence of AgNCs (i.e. the excitation dependence of the low coverage sample should have a slope of 1). The value of 1.51 is the square of the surface field enhancement factor of Hg-light intensity. Thus, by correcting the intensity axis, the slope of the low coverage changes from 0.66 to 1 (a one-photon process). On the same corrected axis, the slope of the high particle coverage changes from 1.33 to 2 (a two-photon process). In effect, the polymer is "experiencing" a much higher intensity of light than what was actually put into the system due to the plasmon field enhancement. After this analysis was carried out, it was obvious that the dependence of the fluorescence intensity on the exciting light was linear at low surface coverage (a one-photon process) and quadratic at high surface coverage (a two photon process).

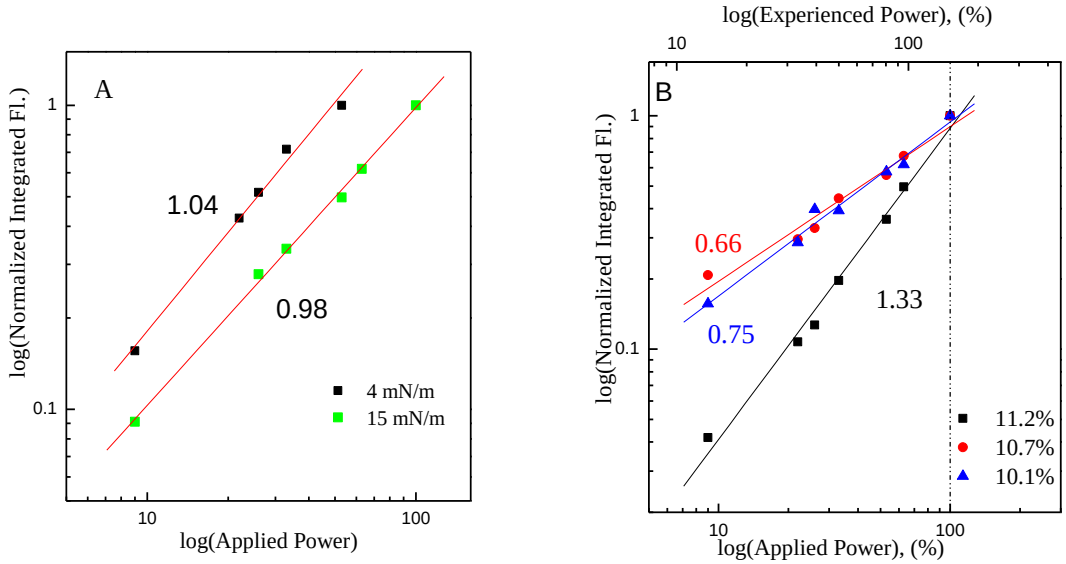

Figure 4.9 Logarithmic plots of the excitation power plotted against the integrated fluorescence intensity of (A) pure polymer samples that were deposited onto quartz substrates at surface pressures of 4 (black) and 15 mN/m (green), as well as (B) PPE fluorescent polymer deposited on the surface of PVP capped AgNC monolayers on quartz substrates at different surface coverage. Samples with 11.2 (black), 10.7% (red) and 10.5% (blue) coverage show altered slopes that indicate the polymer is experiencing fluorescence enhancement in each sample but is undergoing the two-photon process of exciton annihilation in the 11.2% surface coverage sample.

4.4 Conclusions

The intent of this work was to study the interaction of two-dimensional plasmonic nanoparticle arrays with a material that is relevant to current scientific and engineering needs. Conjugated fluorescent polymers are rapidly becoming the focus of the electronics industry, and the effect of enhanced absorption by plasmonic particles can be utilized in many applications. The onset of exciton annihilation in a polymer will need to be considered when constructing these devices so that maximum utility can be drawn from the nanoparticles. This paper also serves to illustrate the potential of plasmonic particles to utilize very low input powers for purposes that normally require large energy densities.

4.5 References

(1) Holzer, W.; Penzkofer, A.; Stockmann, R.; Meysel, H.; Liebegott, H.; Horhold, H. H. Energy density dependent fluorescence quenching of diphenyl substituted phenylene-vinylene and diphenylene-vinylene polymers by exciton-exciton annihilation. *Synth. Met.* **2001**, *125*, 343-357.

(2) Cerullo, G.; Lanzani, G.; De Silvestri, S.; Egelhaaf, H. J.; Luer, L.; Oelkrug, D. Primary photoexcitations in oligophenylenevinylene thin films probed by femtosecond spectroscopy. *Phys. Rev. B: Condens. Matter Mater. Phys.* **2000**, *62*, 2429-2436.

(3) Kepler, R. G.; Valencia, V. S.; Jacobs, S. J.; McNamara, J. J. Exciton-exciton annihilation in poly(p-phenylenevinylene) films. *Synth. Met.* **1996**, *78*, 227-230.

(4) Yan, M.; Rothberg, L. J.; Papadimitrakopoulos, F.; Galvin, M. E.; Miller, T. M. Defect quenching of conjugated polymer luminescence. *Phys. Rev. Lett.* **1994**, *73*, 744-747.

(5) Bunz, U. H. F.; Imhof, J. M.; Bly, R. K.; Bangcuyo, C. G.; Rozanski, L.; Bout, D. A. V. Photophysics of poly [p-(2,5-didodecylphenylene)ethynylene] in thin films. *Macromolecules* **2005**, *38*, 5892-5896.

(6) Shi, Y.; Liu, J.; Yang, Y. Device performance and polymer morphology in polymer light emitting diodes: The control of thin film morphology and device quantum efficiency. *J. Appl. Phys.* **2000**, *87*, 4254-4263.

(7) Mahmoud, M. A.; Tabor, C. E.; El-Sayed, M. A. Surface-Enhanced Raman Scattering Enhancement by Aggregated Silver Nanocube Monolayers Assembled by the Langmuir-Blodgett Technique at Different Surface Pressures. *J. Phys. Chem. C* **2009**, *113*, 5493-5501.

(8) Sun, Y. G.; Xia, Y. N. Shape-controlled synthesis of gold and silver nanoparticles. *Science* **2002**, *298*, 2176-2179.

(9) Siekkinen, A. R.; McLellan, J. M.; Chen, J. Y.; Xia, Y. N. Rapid synthesis of small silver nanocubes by mediating polyol reduction with a trace amount of sodium sulfide or sodium hydrosulfide. *Chem. Phys. Lett.* **2006**, *432*, 491-496.

(10) Mahmoud, M. A.; El-Sayed, M. A. Comparative Study of the Assemblies and the Resulting Plasmon Fields of Langmuir-Blodgett Assembled Monolayers of Silver Nanocubes and Gold Nanocages. *J. Phys. Chem. C* **2008**, *112*, 14618-14625.

(11) Neretina, S.; Qian, W.; Dreaden, E.; Ei-Sayed, M. A.; Hughes, R. A.; Preston, J. S.; Mascher, P. Plasmon field effects on the nonradiative relaxation of hot electrons in an electronically quantized system: CdTe-Au core-shell nanowires. *Nano Lett.* **2008**, *8*, 2410-2418.

(12) Cerullo, G.; Lanzani, G.; De Silvestri, S.; Egelhaaf, H. J.; Luer, L.; Oelkrug, D. Primary photoexcitations in oligophenylenevinylene thin films probed by femtosecond spectroscopy. *Phys. Rev. B* **2000**, *62*, 2429-2436.

(13) Yan, M.; Rothberg, L. J.; Papadimitrakopoulos, F.; Galvin, M. E.; Miller, T. M. Defect Quenching of Conjugated Polymer Luminescence. *Phys. Rev. Lett.* **1994**, *73*, 744-747.

CHAPTER 5

PHOTOPHYSICAL DEPENDENCE OF POLY(PARAPHENYLENEETHYNYLENE) FLUORESCENT POLYMERS ON CHAIN LENGTH AND ASSEMBLY WHEN DEPOSITED AS LANGMUIR-BLODGETT MONOLAYERS OVER SILVER NANOCUBES

Abstract

The photophysical properties of three poly(paraphenyleneethynylene) fluorescent polymers, varying in chain length, were studied as a function of 1) pure polymer surface compression after deposition from a Langmuir-Blodgett trough onto a substrate and 2) deposition of a constant amount of polymer onto the surface of silver nanocube arrays of varying particle densities. The results are discussed in terms of the surface pressure and nanoparticle topography effects on conformation of the fluorescent polymer. It was found that the three polymers each exhibited unique photophysical properties upon compression, requiring individual explanations involving chain length, solubility, and interchain interactions. Each polymer in the nanoparticle/polymer series of experiments exhibited a blue-shift and a substantial narrowing of their emission spectra when deposited on the nanoparticle sample. This effect is presumably a combined effect of conformational changes that shift the emission to higher energy (blue-shift) and plasmonic effects that result in enhancement of primary emission of the polymer (emission from the 0-0 and 1-0 transitions), thus narrowing the emission.

5.1 Introduction

Conjugated polymers, such as the PPE fluorescent polymer presented herein, have been studied extensively to understand and optimize their physical interaction in countless different applications and architectures.[1-3] Spin-casting,[4-5] solution processing,[6-7] and printing processes[8-9] have been developed to apply these polymers to the solid state. Each of these technologies applies the polymeric materials into relatively thick three-dimensional multilayers. Disordered stacking of polymers leads to defects in the materials performance, and many computational and experimental resources have been devoted to understanding the ordering/packing processes that occur for isolated species, two-dimensional, and three-dimensional interactions.[10-13] Two-dimensional films show great promise and are applicable to a wide range of technologies. A very elegant experiment conducted by Swager et. al., demonstrated the photophysical effects of PPE monolayers that were compressed as floating monolayers cast over the surface of water.[14] This allows for investigation of the more "ideal" monolayer compared to the monolayer after it is deposited onto a solid surface of interest, which may be far from "ideal." The purpose of this chapter is to more deeply investigate the photophysical effects of the monolayers once they have been deposited onto a solid architecture of interest. Three polymers of different lengths are first deposited onto the surface of glass substrates at varied surface pressures. The polymers are also deposited over the surface of nanoparticle arrays. The effect of surface pressure, coupled with the different architectures, is studied spectroscopically by absorption and emission measurements of the deposited monolayer films.

5.2 Experimental

5.2.1 Reagents and Solvents

ACS reagent grade silver nitrate, polyvinyl pyrolidone (MW = 55,000), anhydrous ethylene glycol, and spectrophotometeric grade chloroform were obtained from Sigma Aldrich (St. Louis, MO). $AgNO_3$ solutions were made 15 minutes prior to addition to avoid oxidation by EG. Reagent grade sodium sulfide nonahydrate was purchased from MP Biomedicals (Solon, OH). The 3 mM sodium sulfide solution was made fresh through serial dilution of a 30 mM stock solution. Reagent grade methanol and acetone were purchased from BDH Middle East (Dubai, UAE)

5.2.2 Silver Nanocube Synthesis

The method of Sun and Xia was used with slight modification to synthesize silver nanocubes (AgNCs).[15-16] To begin, 35 mL of ethylene glycol (EG) was slowly stirred and heated in a 100 mL round-bottom flask at 140 to 150^{o}C for 1 hour. After 1 hour of heating, 5mL of polyvinyl pyrrolidone (PVP) (0.08 g/mL in EG; MW ~55,000) was added to the hot EG solution. The temperature of the reaction mixture was then gradually increased to 155^{o}C. At this temperature, 0.4 mL of sodium sulfide solution (3 mM in EG) was added followed by 2.5 mL of $AgNO_3$ solution (0.096 g/mL in EG). The color of the reaction mixture changed from transparent yellow, after adding the $AgNO_3$ solution, to an opaque green-yellow at the end of the reaction. AgNCs were cleaned from the EG solvent and excess PVP capping material by dilution of 10 mL of AgNCs solution with 20 mL deionized water and centrifugation for 5 minutes at 13,000 rpm. The precipitated AgNCs were then dispersed in 5 mL chloroform for use on the LB trough.[17]

5.2.3 PPE Polymer Preparation

The poly(paraphenyleneethynylene) fluorescent polymers were made by Jonathan Bryant in the laboratory of Uwe Bunz. The basic synthesis of the PPE fluorescent polymers is discussed in detail within Appendix A. The details of creating the varying lengths of polymers is not contained within this thesis.[18]

5.2.4 Langmuir-Blodgett Deposition of AgNCs and PPE Fluorescent Polymer

Assembly of particle and polymer monolayers was carried out on a Nima 611-D Langmuir-Blodgett trough. The surface pressure of each monolayer was monitored with a D1L-75 model surface pressure sensor. To begin, the available surface area of the trough was adjusted to 500 cm^2. Then, 0.5 mL of AgNCs in chloroform was sprayed over the surface of the water sub-phase of the trough using a micro syringe. The AgNC monolayers were transferred onto the surface of glass or silicon-wafer substrates, at surface pressures of 0.0, 0.2, 0.5, 1.0, 3.0, 5.0, 6.0, and 8.0 mN/m by the vertical dipping method. In order to apply PPE monolayers to the surface of AgNCs, the PPE samples were dissolved in chloroform, sprayed over the surface of water, and the monolayers were deposited over AgNC monolayers at a constant surface pressure of 0.1 mN/m for each sample. For the pure PPE experiment, the polymers were compressed to surface pressures of 1.0, 5.0, 8.0, 10.0, 12.0, 15.0, and 20.0 mN/m. Absorbance and steady-state fluorescence measurements were taken with an Ocean Optics HR4000Cg-UV-NIR absorption spectrometer and a Craic 100 microfluorescence spectrometer, respectively. Images were taken on a Zeiss Ultra60 SEM (scanning electron microscope) to determine the size, monodispersity, and percent surface-coverage of the particles. SEM images are showed in Figures B.4-B.11 in Appendix B.

5.3 Results and Discussion

5.3.1 Optical properties of pure PPE with different polymer density and chain length

The optical properties of π-conjugated polymers greatly depend on the geometric conformation of the polymer backbone. Conformations that extend conjugation lead to a red-shift in the absorption spectrum, due to the generation/shifting of electronic and vibronic energy levels to lower energy. The changes in the electronic structure of the π-conjugated polymer also lead to changes in its emission characteristics. For this reason, the ultimate efficiency of polymer devices, such as solar cells, greatly depend on the geometric conformation and assembly of their intrinsic polymer constituents. It has been reported that the geometric conformations of π-conjugated polymers can be substantially affected by compression on the surface of an LB trough, and those changes in structure have been recorded spectroscopically.[14] The floating monolayer represents an ideal situation for formation and control. For most practical applications, the π-conjugated polymers must be utilized on a solid substrate. The transfer from the surface of the water sub-phase of the LB trough to a "less than ideal" substrate should cause changes to the optical properties (absorption and fluorescence emission). Herein, we aim to elucidate the structural changes of the PPE fluorescent polymers of varied chain length when compressed to different surface pressures. In order to probe real-world application of these monolayers, all measurements were conducted on samples after deposition of the polymer onto a substrate of interest. Absorption and fluorescence spectroscopy are used for insight into the geometric changes and electronic interactions caused by increasing surface pressure.

5.3.1.1 Effect of monolayer compression on the optical properties of deposited PPE15 polymer

Figure 5.1A shows the normalized absorption spectra of PPE15 (n = 15) as deposited on a glass substrate at surface pressures ranging from 1.1 to 19.9 mN/m. The normalized absorption and emission spectra are presented to compare the fine differences between each spectrum. A slight red-shift (454 to 459 nm) and broadening (FWHM, 61 to 68 nm) can be seen in the absorption spectra as the surface pressure increases. The emission spectra (Figure 5.1B) show similar behavior; a red-shift from 474 to 482 nm and FWHM broadening from 71 to 78 nm with increasing pressure. It is not unusual for PPE polymers to have broad absorbance spectra in a good solvent, e.g. chloroform, because they have low ground state torsional barriers around the backbone of the polymer (Figure B.1-B.3). The sharpness of the absorption peak in the inset of Figure 5.1 signifies the universal restriction of the rotational coordinate of this polymer when it is deposited on a solid support. The excited-state of PPE polymers is normally associated with a very deep potential-well that is caused by the formation of a cumulenic structure that restricts free-rotation to a select few conformations. This restriction is routinely visible as a sharp emission profile when dissolved in a good solvent, such as chloroform, that ensures polymer chains act as isolated species.[19-21] The broadening seen in the emission spectrum in Figure B.1 is caused by water-induced aggregates that restrict rotation of the polymer backbone from its optimal geometry.[22] The emission of the PPE polymer is typically so sharp that any deviation from that optimal structure will broaden the spectral profile. This is analogous to the restriction of rotation when the polymer is deposited or brought into close contact with adjacent polymers (packing) by the LB method.

The narrow absorbance and emission bands suggest a tight distribution of conformations that are restricted from obtaining optimal geometric configuration in the ground and excited states. The broadening of the emission band with increasing surface pressure, coupled with slight red-shifting of the spectra to lower energies, can be caused by increased interchain interactions such as energy transfer, excimers, or π-π interactions.[13-14,23] Dielectric and conformational changes with pressure are probable and will subtly affect spectra. Given that the spectra do not dramatically change with surface pressure, it seems that energy transfer or π-π interactions are limited.

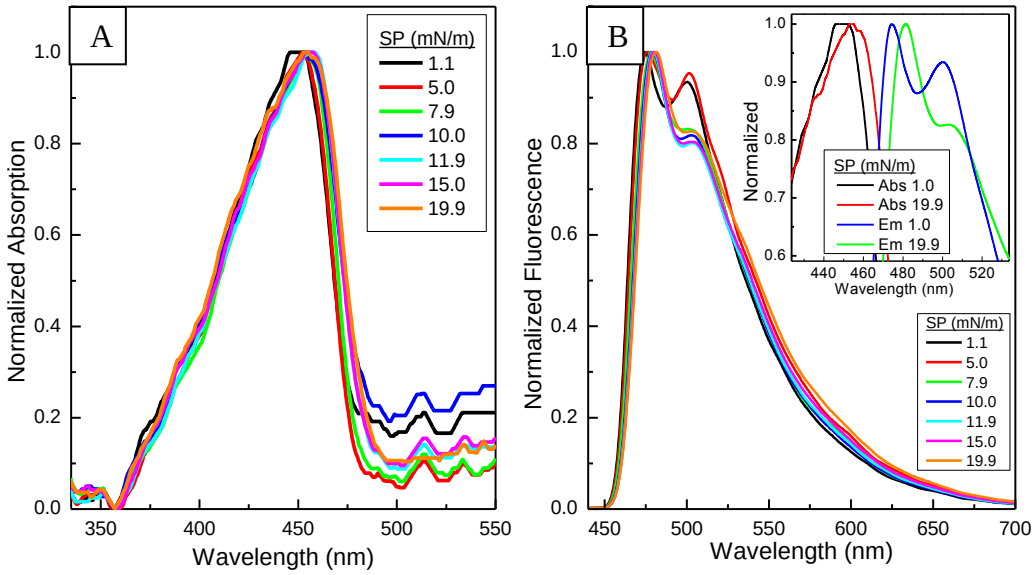

Figure 5.1: (A) Absorption and (B) emission spectra of PPE15 fluorescent polymer compressed at a range of different surface pressures, varying from 1.1 (black) to 19.9 mN/m (orange). The absorption peak maxima shifted correspondingly from 454 to 459 nm and the FWHM broadened from 61 to 68 nm. Within the emission spectra, the higher energy peak shifted from 474 to 482 nm and the FWHM broadened from 71 to 78 nm. A distinct low-energy peak becomes much less prominent after the surface pressure is increased from 5.0 to 7.9 mN/m, which may indicate a change in the structure that causes the lower energy transition to become less probable. (C) Overlaid absorption and emission spectrum of PPE15 at surface pressures of 1.1 and 19.9 mN/m.

5.3.1.2 Effect of monolayer compression on the optical properties of deposited PPE25 polymer

In stark contrast to PPE15, deposited PPE25 (n = 25 repeat units) shows a significant amount of response to the increased surface pressure applied by the LB trough. Figure 5.2 (A & B) shows the absorption and emission spectra of PPE25 as the surface pressure is increased from 0.9 to 19.9 mN/m. Again the overlaid absorption and emission spectra of the 0.9 and 19.9 mN/m samples are shown in the inset of Figure 5.2B. The absorption spectra show a clear broadening (FWHM: 77 to 95 nm), but the peaks remain centered around the same wavelength (4 nm red-shift, 436 to 440 nm) throughout the surface pressure range. Interestingly, the broadening seems to occur only to the red side of the peak. As with PPE15, this broadening may be attributed to substantial increases in the geometric distribution in the ground state as the surface pressure increases. It is also possible that the broadening of the peak to the red, without significant change in the peak maxima, indicates the onset of a new peak around 470 nm, which often indicates the presence of π- π interactions.[14,24] Considering the fluorescence spectra of Figures 2 (B) and (C), which show a large red-shift from 498 to 540 nm and a substantial increase in the FWHM (84 to 121 nm), there are obvious increases in interchain interactions with increases in surface pressure. The appearance of a large (broad) emission is indicative of increases in one or multiple interchain interactions via an energy transfer process, the formation of an excimer, and/or by low-energy pi-pi stacking interactions. It is interesting to note that the emission of the 0.9 mN/m sample resembles the solution spectrum in Figure B.2, in the supporting information, but the peak shape differs significantly. This lends additional support to the notion that the

PPE25 polymer is experiencing some interchain interactions at the lowest surface pressure.

Excimer species exist as the interaction of a ground state species with an excited state species, and usually occur without change in the absorption spectrum. Also, excimer emission is usually very broad, which is the case to some extent.[22,25] The onset of a red-shifted peak in the absorption spectra would suggest a ground state interaction, potentially induced by π-π overlap if the polymer backbones can be oriented in such a way. This sort of overlap usually requires a disordered three dimensional system (e.g. spin coating) in-which the polymer backbones can lay perpendicular on top of one another.[23] This orientation is unlikely since the isotherms for this polymer indicated only marginal signs of monolayer breaking at the highest surface pressure (19.9 mN/m). Swager et. al. demonstrated[14] that a monolayer of polymer with hydrophobic side-chains can be designed to cause the aromatic rings to stack perpendicular to the surface of water at low or intermediate surface pressures. The π-π stacking of polymer aromatic rings seems like an attractive explanation given the potential onset of a red-shifted peak in the absorption and the broadened emission. In Swager's work, an exceptionally large red-shifted peak in the absorption spectra and an extremely broad low-energy emission were present from the π-π stacking. These cues are not blindingly obvious in this data, but contributions from these interactions may be occurring.

Energy transfer from high energy structures to the new low energy structures are made possible from partial planarization of phenyl rings that occurs during the compression and deposition procedures, and are very likely a primary cause of the spectral observations. This process would lead to broadened absorption and

broadened/red-shifted emission spectra. Energy transfer is the simplest explanation, and as a result it is the most likely (Occam's Razor). It is probable that there are additional contributions from excimer and π-π interacting chains occurring within the population that convolute the spectra and suggest, but do not confirm, their presence.

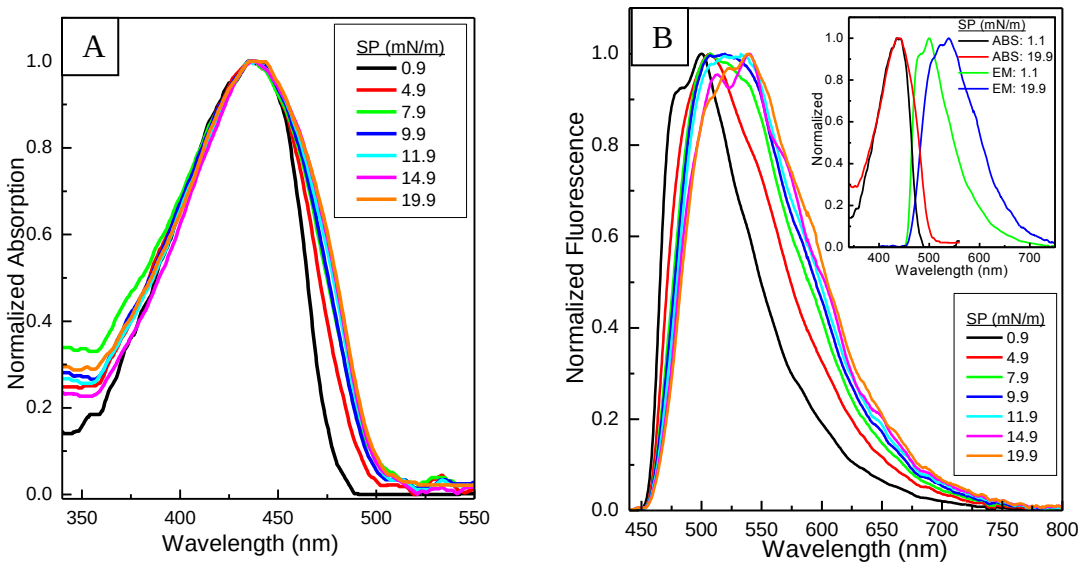

Figure 5.2: (A) Absorption and (B) emission spectra of PPE fluorescent polymer PPE25 compressed at a range of different surface pressures varying from 0.9 (black) to 19.9 mN/m (orange). The absorption peak maxima shifted correspondingly from 436 to 440 nm and the FWHM broadened from 77 to 95 nm. The peak structure of the emission spectra changes rapidly from well-defined to relatively featureless and then regains some of its structure; shifting from 498 to 540 nm and broadening from 84 to 121 nm FWHM. Although the absorption spectra do not shift significantly, the large degree of broadening in the Absorption and emission spectra signify a large range of optically active conformations and interactions. (C) Overlaid absorption and emission spectrum of PPE25 with surface pressure of 0.9 and 19.9 mN/m.

5.3.1.3 Effect of monolayer compression on the optical properties of deposited PPE36 polymer

Figure 5.3 (A & B) shows the absorbance and emission spectra of PPE36 (n = 36 repeat units). Interestingly, PPE36 exhibits a blue-shift of the absorption peak with

increasing surface pressure (443 to 434 nm). In addition to the blue-shift, the peak broadens from 70 to 98 nm. The blue-shifted spectra are indicative of a significant amount of disorder or strain that would cause the ground-state species to exist at higher energy configurations. It is possible that the polymer chains may adopt less than linear geometries (folded or bent). An increase in surface pressure may cause additional deviations from the lowest energy state; the conjugation of the extended polymer chain may be broken. In such cases the polymer will behave as if it were two independent oligomers, which are known to have higher energy absorption values than polymers.[19-20]

Again, the lowest (0.9 mN/m) and highest (20.0 mN/m) surface pressure samples are overlaid in the inset of Figure 5.3B. The emission from PPE36 red-shifts from 500 to 511 nm and the spectra broaden from 87 to 100 nm. The generation of multiple oligomeric excited states would certainly result in broadened emission and some band structure (typical of oligomer species) may be imparted to the overall spectrum. It seems logical that if this were the case, the emission would then broaden to the blue side of the peak as pressure increased (consistent with the formation of higher energy oligomers). In fact, we see the opposite behavior. There is a blue-shoulder that exists for samples up to 5.0 mN/m and is then lost with increasing pressure. The significant amount of red-shifting and broadening would suggest that there is a large distribution of configurations present within the population of emitting species. This does not mean that these high energy oligomeric species do not exist. It seems likely that with the additional interchain interaction that is caused by increased surface pressure, energy transfer from these high energy oligomeric species to low energy polymeric species would become prominent. If

energy transfer is occurring, as just described, the disappearance of the high energy emission peaks (blue shoulder) in Figure 3B are easily explained.

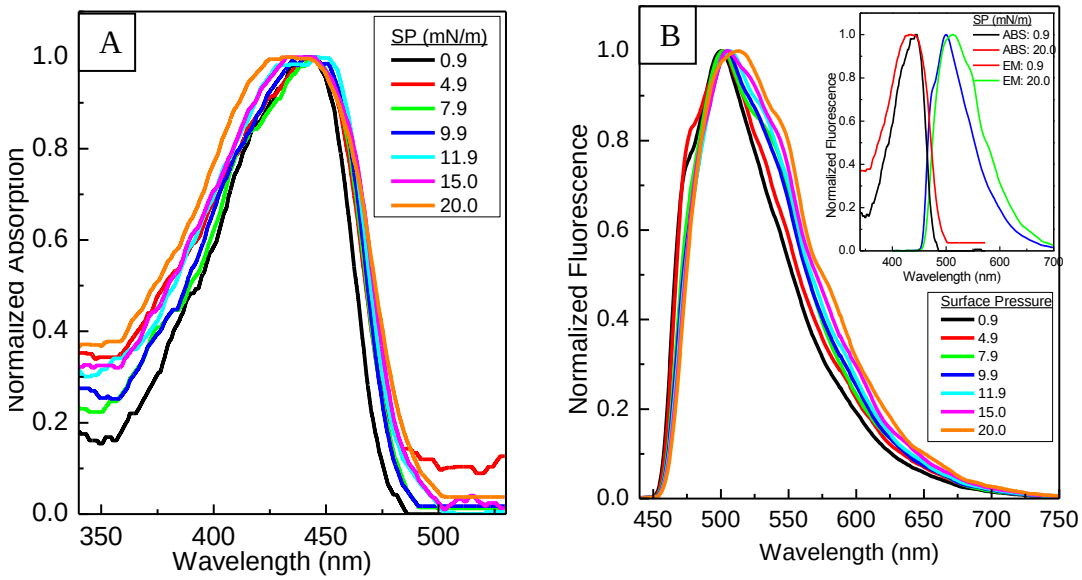

Figure 5.3: (A) Absorption and (B) emission spectra of PPE fluorescent polymer PPE36 compressed at a range of different surface pressures varying from 0.9 (black) to 20.0 mN/m (orange). In contrast to previous samples, the absorption peak maximum blue-shifted from 443 to 434 nm and the FWHM broadened from 70 to 98 nm with increasing surface pressure. The structure of the emission spectra show a shoulder on the high-energy side of the main peak that disappears with increasing surface pressure. The emission peak maximum shifted from 501 to 512 nm and broadened from 87 to 100 nm FWHM. The blue-shift in the absorption spectra strongly indicates a general decrease in conjugation, which may be giving rise to higher energy spectral properties of oligomeric species of PPE. Along with the blue-shift, the large degree of broadening supports the idea of a vast array of configurations, which include oligomeric and polymeric species of different geometries which broaden and red-shift the emission. (C) Overlaid absorption and emission spectrum of PPE36 with surface pressure of 0.9 and 20 mN/m.

5.3.1.4. Comparison of the optical properties of PPE polymers of different chain length.

The substantial factor that distinguishes PPE15 from the other two polymers is that the absorption and emission profiles remain unchanged through the entirety of the compression range (1.1-19.9 mN/m). Both absorption and emission remain narrow and

show only marginal peak shifting (Figure 5.4). It is actually remarkable that the polymer structure stays in its "isolated" state (does not exhibit interchain interactions) at such high surface pressures. This feature, unique to PPE15 within the scope of this work, could occur or be aided by the charged side-chains which may help to electrostatically isolate the fluorescent backbone from intimate contact. Each of the polymers tested in this paper should have the same electrostatic advantage, given that they were synthesized to be the same. In contrast to the other polymers, "isolation" of PPE15 may be made easier because the polymer is short and most likely does not flex or bend nearly as much as the longer polymer chains.[26]

PPE25 distinguishes itself with nearly the complete opposite behavior of PPE15. As seen in Figure 5.4 and discussed above, PPE25 responds immediately to pressure increases with strong red-shifting and broadening of the emission. The absence of peak-shifting in the absorbance and the emergence of an additional red-shifted peak seem to suggest that the emission characteristics are due to new ground state and excimeric species. Given that preliminary observations demonstrated a greater degree of hydrophobicity in PPE25, compared to the other two polymers, the behavior of the polymer in a film seems most likely to be due to incomplete functionalization of the amine group or excessive defects that exposed unfunctionalized hydrophobic side-chains and/or the hydrophobic backbone, and ultimately result in a polymer that is less soluble in water. A polymer with low solubility, such as the case with PPE25, could initiate alternate arrangements (such as π-π interactions) that are not possible in the other polymers because their hydrophilic side chains interact strongly with the water subphase.

This could explain the emergence of a new ground-state peak at lower energies and the broadened emission without a substantially broadened absorption or peak shifting.

Of the polymers already discussed, PPE36 is the only polymer that exhibits a blue-shift of the absorption peak. The value shown in Figure 5.4 does not reflect the blue-shift as a negative value, but simply as an absolute change in peak shift. The behavior of PPE 36 appears to lie somewhere in between PPE15 and PPE25. The polymer obviously responds to the increasing surface pressure with changes to the peak maximum and FWHM for both ground and excited state, which is in contrast to PPE15. At the same time, PPE36 does not show any of the markers for π-π or excimer interactions that were discussed for PPE25. The substantial increase in the FWHM, in addition to the blue-shifting of the absorption peak, could indicate the formation of high energy oligomers that are only present in the longest polymer chain, because of its higher susceptibility to pressure induced conformational bending and/or breaking of the conjugation.

Ultimately, the sensitivity of construction and utilizing conjugated polymer species has been demonstrated here. Three polymers of different chain lengths have exhibited three unique sets of photophysical properties as the monolayer density was increased through surface pressure. PPE15 shows little effect from the increased surface pressure, while PPE25 and PPE36 both experience interchain interactions in their own unique ways. The appearance of π-π stacking interactions of PPE25 was unexpected and is most likely the result of working with a more hydrophobic polymer. The reason behind the hydrophobic nature has been speculated to be due to incomplete functionalization and/or the presence of defects in the polymer structure that exposes hydrophobic backbone of the polymer. Lastly, the blue-shifting of the absorption of PPE36 seem most

likely due to the formation of high energy oligomers induced by conformational breaking of the conjugation.

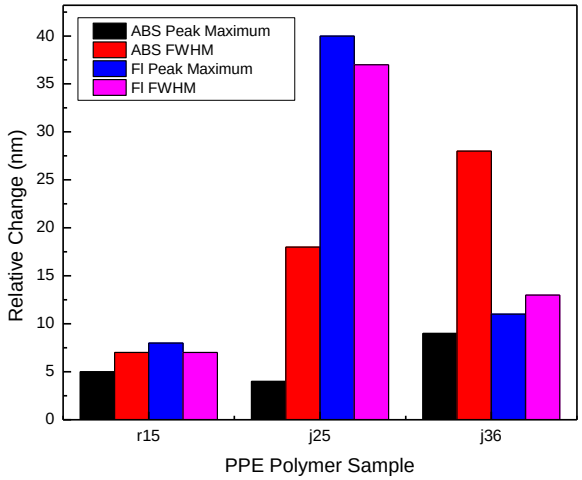

Figure 5.4: Absolute change in the peak maximum and FWHM expressed in nanometers (nm) for the absorption and emission spectra of PPE15, PPE25, and PPE36 as the polymers were compressed from 1 to 20 mN/m. The shift in the absorption maximum for PPE36 resulted in a blue-shift, in contrast the red-shifting of PPE15 and PPE25.

5.3.1.5 Optical properties of pure PPE polymer with different chain length

Plasmonic nanoparticles have been used to enhance the optical properties (e.g. absorption and emission) of many materials. Although the nanoparticles will alter the optical properties of the polymer material through plasmonic interaction, they might also change the conformation of the polymer. This will also affect both the absorption and emission of the polymer. In the former section we showed the effect of surface pressure on the optical properties of PPE polymers with different chain length, and explain the results through changes to the polymer conformation. In this section the optical properties of PPE monolayers that have been deposited over an AgNC array is investigated. The AgNCs are assembled into a monolayer at different surface pressures, and the polymer

monolayer coats that AgNC array at a small constant surface pressure (0.1mN/m). In this case, the PPE monolayer is no longer interacting with a flat topography. Instead, the film is in contact with relatively large structures (~50-60 nm) and the polymer must react to the physical nature of these features.

The purpose of this study is to monitor the effect of nanoparticles on the conformation of the PPE polymer as well as consider the plasmonic effect of the nanoparticles on the optical properties of the PPE polymer. In order to limit the effect of interchain interactions inherent in the deposited monolayer of PPE, discussed in the former section, the surface pressure of the PPE polymer was chosen to be low (0.1 mN/m).

As the PPE fluorescent polymer is deposited over unique structures, such as nanoparticle architectures, several interactions can be expected under varying conditions. It has been established in the literature that plasmonic nanoparticles can alter the absorption and emission characteristics of photoactive systems within its field of influence.[27-28] This can be achieved through nonradiative quenching of emission if contact is within ~ 5 nm, or they can enhance radiative effects through dipolar interactions with the plasmonic field at larger distances where quenching is lessened.

Roughly speaking, the average length of each polymer (estimated by ChemBio 3D Ultra, assuming a linear configuration) would be approximately 20, 33, and 48 nm for the PPE15, PPE25, and PPE36, respectively. The dimension of the AgNCs that the polymer monolayers are deposited over is 52 ± 6 nm. For larger polymers, such as PPE36, there is an increasing chance that the polymer will extend over the edge of a nanocube. Deformation of the polymer chain could lead to decreased conjugation, and

breaking of conjugation could cause the appearance of spectral contributions from the oligomer species.[19-20] These occurrences could also lead to an interesting possibility in which the polymer backbone (the fluorophore) is positioned parallel to the exciting light where the chance of excitation is minimal. The disruption of the ordered polymer monolayer-packing by the nanoparticle array will affect the planarization and linearity of the polymer backbones, as well as the dielectric environment around the polymer.

5.3.2 Effect of AgNC surface pressure PPE fluorescent polymers of different chain length

5.3.2.1 Effect of AgNC surface pressure on the optical properties of PPE15

The spectra of PPE15 samples prepared though deposition of the polymer monolayer (at a constant surface pressure) over AgNC monolayers that were deposited at different surface pressures are shown in Figure 5.5A. A low surface pressure (0.1 mN/m) was chosen for the deposition of the polymer in order to avoid some of the potential convoluting effects that were caused by increased surface pressure in Section A. The optical density of AgNC monolayers increases as surface pressure is increased. Additionally, the SPR peak position of AgNCs red-shifts with increased surface pressure, due to plasmon coupling. The inset of Figure 5.5A shows the absorption spectrum of pure PPE15, PPE25, and PPE36 monolayers. The normalized emission spectra of PPE15 (Figure 5.5B) shows an obvious decrease in the FWHM from the pure polymer (76 nm, black) to the AgNC incorporated samples (FWHM: 68-66 nm with increasing surface pressure). A corresponding initial blue-shift of the peak maximum of the pure polymer, at 497 nm, to the lowest surface pressure PPE/AgNC sample, at 495 nm, was observed and followed by the additional blue-shifting to 493 nm as the surface pressure increased to its highest value. The inset of Figure 5.5B shows a scatter plot of the integrated fluorescence

for each spectrum as a function of surface pressure, calculated prior to normalization. It is clear that the emission undergoes an initial increase from pure polymer to the AgNC-incorporated samples, but the emission intensity levels off shortly thereafter. Small deviations occur in the height of the 472 nm peak/shoulder compared to the 500 nm peak, but they are highly erratic.

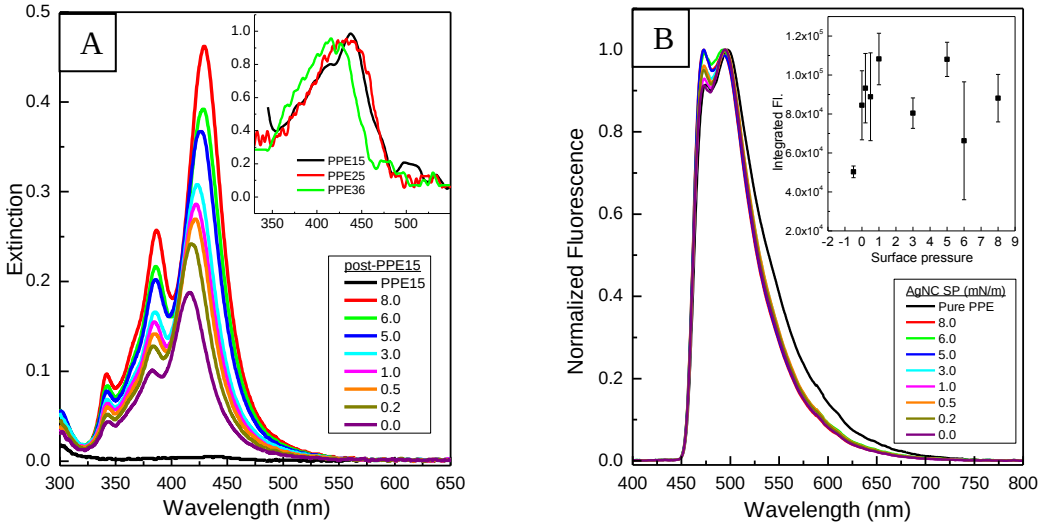

Figure 5.5: (A) Extinction of PPE15 deposited at constant surface pressure (0.1 mN/m) over the surface of AgNCs of varied nanoparticle surface pressure. The AgNC extinction peak intensity and peak position increase and red-shift, respectively, with increasing surface pressure. (A, inset) Absorption spectra of the pure PPE15, PPE25, and PPE36 samples assembled on the surface of glass substrates at a surface pressure of 0.1 mN/m. (B) Emission of pure PPE15 blue-shifts from 497 to 493 nm when the AgNCs are introduced at the lowest surface pressure (purple). Likewise, the FWHM of pure PPE15 narrows from 76 to 68 nm at the lowest surface pressure. There is a small blue-shift and narrowing as the surface pressure of the AgNCs is increased (~2 nm in each case). Slight fluctuations in the peak/shoulder at 472 nm may be related to conformation. (B, inset) Scatter plot of the integrated fluorescence, prior to normalization, as a function of surface pressure.

5.3.2.2 Effect of AgNC surface pressure on the optical properties of PPE25

Figure 5.6A shows emission data of PPE25. Extinction spectra, which are nearly identical to those shown in Figure 5.5A, are contained in Figure B.12. The absorption of the pure polymer is shown as a red trace in Figure 5.5A and is very small compared to the nanoparticles. Again, the emission of the pure PPE sample is lower energy (λ_{max} = 500 nm) and exhibits a much broader FWHM (92 nm) compared to the AgNC samples, which blue-shift (from 495 to 491 nm) and narrow (83 to 73 nm) as AgNC surface pressure increases. Interesting in the case of PPE25, is a significantly less structured emission spectrum compared to PPE15, which would suggest a greater distribution of emissive transitions. This appears to be inherent to the polymer itself, because the observation is constant through pure PPE25 and AgNC/PPE samples. The inset of Figure 5.6A shows a significant increase in emission from the pure polymer compared to the highest pressure PPE/AgNC sample.

5.3.2.3 Effect of AgNC surface pressure on the optical properties of PPE36

The spectra of the last polymer in the series, PPE36, are shown in Figure 5.6B. The inset of Figure 5.6B shows similar behavior to PPE25. A significant increase in the integrated fluorescence with increased surface pressure is observed. Like the previous polymers, the spectra of PPE36 blue-shifts; from 498 nm of the pure polymer to 496 nm at the lowest AgNC surface pressure, and 492 nm at the highest surface pressure. The FWHM of the spectral profiles narrow from 83 nm (pure polymer PPE36) to 74 nm at the lowest surface perssure. After increasing the AgNC surface pressure to its highest value, the profile continues narrowing to 70 nm. The exceptional part of this spectral evolution is that after the particles are deposited over the lowest surface pressure of AgNCs, a blue-

shoulder begins to appear in the emission profile (470 nm). With increased surface pressure of AgNCs, the shoulder becomes prominent. The evolution of this blue shoulder into a peak, with increasing surface pressure, is in direct opposition to the observation of the pure polymer in Figure 5.2B, in which the blue-shoulder/peak disappears with increasing surface pressure.

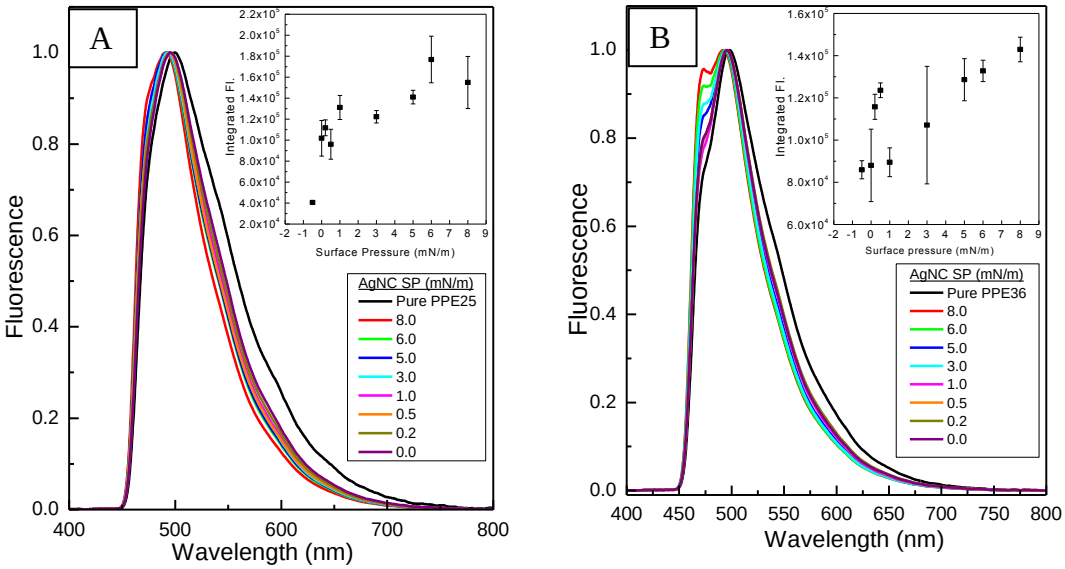

Figure 5.6: (A) Emission spectra of the pure polymer PPE25 blue-shifts from 500 to 495 nm at the lowest surface pressure PPE/AgNC sample, after which a blue-shift of and additional 4 nm is observed at the highest AgNC surface pressure. The FWHM changes significantly from pure polymer (92 nm) to the lowest AgNC surface pressure (83 nm, purple). As the surface pressure of the particle is increased to its maximum, the FWHM narrows to 73 nm. (A, inset) Large increase in emission from pure PPE PPE25 to the highest surface pressure are observed. (B) The emission of the pure polymer PPE36 blue-shifts from 498 to 496 nm upon introduction to the lowest surface pressure of particles, after which a blue-shift of 4 nm is observed to the highest surface pressure. The FWHM of the pure polymer narrows from 83 to 74 nm at the lowest surface pressure of particles. After increasing particle surface pressure, the FWHM narrows to 70 nm. (B, inset) An initial increase in integrated fluorescence with increasing nanoparticle surface pressure is observed.

5.3.2.4 Comparison of the effects of AgNC surface-pressure on PPE polymers of different length

The most interesting features that are present in each of the PPE/AgNC series of experiments are the overall blue-shifts in the emission and a general narrowing of each emission spectrum from pure polymer to the highest surface pressure of AgNCs. The trends shown in Figure 5.7 are absolute values, but each corresponds to a blue-shift or a peak narrowing. Across all polymers, the most substantial and consistent spectroscopic occurrence was an 8-9 nm narrowing of the FWHM from the pure polymer to the lowest surface pressure of AgNCs (Figure 5.7, blue). Following this initial band narrowing, the trend continues as the surface pressure is increased from 0.0 to 8.0 mN/m AgNC (Figure 5.7, magenta), but to varying extents. The narrowing was marginal for PPE15 and PPE 36 (2-4 nm), but PPE25 exhibited an additional 10 nm decrease to the FWHM. Overall the peak maxima for each of the polymers does not shift significantly, but a blue-shift is persistent in each polymer (Figure 5.7, blue/red).

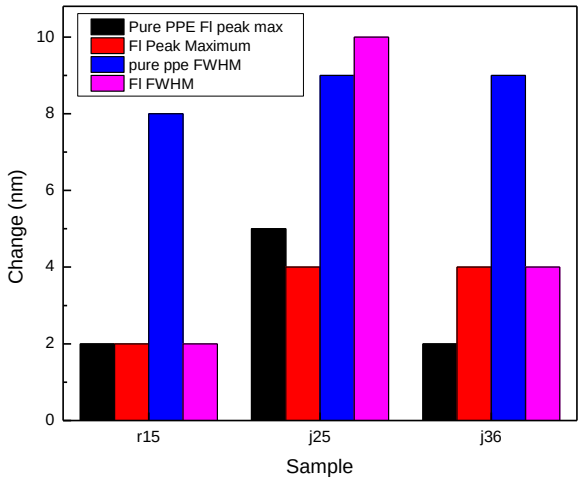

Figure 5.7: Relative change in the peak maximum and FWHM (nm) for the emission spectra of PPE15, PPE25, and PPE36. The change in peak maximum (FWHM) from the pure polymer sample to the 0.0 mN/m surface pressure PPE/AgNC sample is shown in black (blue). The relative change in peak maximum (FWHM) from the 0.0 mN/m PPE/AgNC sample to the 8.0 mN/m PPE/AgNC sample is shown in red (magenta). All data shown above are reported as absolute values of the shift. Each value indicates a blue-shift in peak maximum or a narrowing of the FWHM by the given value.

It seems counterintuitive to suggest that depositing PPE fluorescent polymers over the surface of a disordered array of AgNCs would cause an organizing or unifying effect in the polymer emission spectrum. If additional conformations or interaction were introduced by AgNCs, a large broadening would be expected. However, this is not the case. The substantial narrowing of emission of the pure polymer, whose initial FWHM differs little from that seen from its counterpart in section A, does indeed indicate that the distribution of conformations of the emissive population is smaller. As suggested by the previous statement, AgNCs may be promoting emission from a small sample of conformations existing among those of the greater population. The fact that the polymer spectra are simultaneously blue-shifting and narrowing suggests that those lower energy

conformations are no longer present or are simply being overshadowed by the amplified emission from high-energy conformations.

Plasmonic particles are known to enhance emission of nearby fluorophores. The insets of Figures 5 and 6 clearly show enhancement of the emission from each PPE polymer once it has been deposited on the surface of AgNCs. It is possible that AgNCs have only affected the PPE conformations in their local environment and are simultaneously enhancing the emission of that proximal population and overshadowing lower energy emissive states from polymers beyond the influence of the nanoparticle. This process would result in a narrowing and a blue shift of the emission. Additionally, high probability transitions, such as the 0-0 and 0-1 emissions seen as the prominent peaks in all spectra within this work, could be enhanced by the plasmonic field to a larger degree simply because they occur more often naturally. The observed blue-shifting and narrowing may simply be a natural response to the amplified absorption process initiated by the plasmonic field.

5.4 Conclusions

As stated previously, the purpose of this series of experiments was examine the photophysical effects of PPE fluorescent polymer monolayers once they have been deposited onto a solid material of interest. By examining each fluorescent polymer through its full range of compression, an understanding of the fundamental properties of each polymer/chain length was established. The three polymers each exhibited unique photophysical properties upon compression that required consideration of chain length, solubility, and interchain interactions. These observations provided a starting point for the interpretation of the spectra of the PPE polymer deposited over the surface of AgNCs.

Each polymer in the nanoparticle/polymer series of experiments exhibited an unexpected blue-shift and a substantial narrowing of their emission spectra when deposited on nanoparticle samples of increasing surface pressure. This effect is presumably a combined effect of conformational changes that shift the emission to higher energy (blue-shift) and plasmonic influence. The shifting of emission to higher energy may be due, in part, to destabilization of the polymer through bending and deformation over the AgNC topography. Additionally, the plasmonic fields may simply result in enhancement of primary emission (emission from the 0-0 and/or 1-0 transitions) of the polymer over high-order vibronic transitions, thus narrowing the emission. If 2D polymer films, such as the PPE fluorescent polymer monolayers, are to be used optimally in practical devices, experiments such as these are required to fully understand the interactions of individual constituents.

5.5 References

(1) Grimsdale, A. C.; Chan, K. L.; Martin, R. E.; Jokisz, P. G.; Holmes, A. B. Synthesis of Light-Emitting Conjugated Polymers for Applications in Electroluminescent Devices. *Chem. Rev.* **2009**, *109*, 897-1091.

(2) Cheng, Y. J.; Yang, S. H.; Hsu, C. S. Synthesis of Conjugated Polymers for Organic Solar Cell Applications. *Chem. Rev.* **2009**, *109*, 5868-5923.

(3) Thomas, S. W.; Joly, G. D.; Swager, T. M. Chemical sensors based on amplifying fluorescent conjugated polymers. *Chem. Rev.* **2007**, *107*, 1339-1386.

(4) Shi, Y.; Liu, J.; Yang, Y. Device performance and polymer morphology in polymer light emitting diodes: The control of thin film morphology and device quantum efficiency. *J. Appl. Phys.* **2000**, *87*, 4254-4263.

(5) Jaczewska, J.; Budkowski, A.; Bernasik, A.; Raptis, I.; Moons, E.; Goustouridis, D.; Haberko, J.; Rysz, J. Ordering domains of spin cast blends of conjugated and dielectric polymers on surfaces patterned by soft- and photo-lithography. *Soft Matter* **2009**, *5*, 234-241.

(6) Muller, C. D.; Falcou, A.; Reckefuss, N.; Rojahn, M.; Wiederhirn, V.; Rudati, P.; Frohne, H.; Nuyken, O.; Becker, H.; Meerholz, K. Multi-colour organic light-emitting displays by solution processing. *Nature* **2003**, *421*, 829-833.

(7) Arias, A. C.; Corcoran, N.; Banach, M.; Friend, R. H.; MacKenzie, J. D.; Huck, W. T. S. Vertically segregated polymer-blend photovoltaic thin-film structures through surface-mediated solution processing. *Appl. Phys. Lett.* **2002**, *80*, 1695-1697.

(8) Yan, H.; Chen, Z. H.; Zheng, Y.; Newman, C.; Quinn, J. R.; Dotz, F.; Kastler, M.; Facchetti, A. A high-mobility electron-transporting polymer for printed transistors. *Nature* **2009**, *457*, 679-U671.

(9) Tekin, E.; Holder, E.; Kozodaev, D.; Schubert, U. S. Controlled pattern formation of poly 2-methoxy-5(2 '-ethylhexyloxyl)-1,4-phenylenevinylene (MEH-PPV) by ink-jet printing. *Adv. Funct. Mater.* **2007**, *17*, 277-284.

(10) Leclere, P.; Surin, M.; Brocorens, P.; Cavallini, M.; Biscarini, F.; Lazzaroni, R. Supramolecular assembly of conjugated polymers: From molecular engineering to solid-state properties. *Mater. Sci. Eng. R-Rep.* **2006**, *55*, 1-56.

(11) Cornil, J.; dos Santos, D. A.; Crispin, X.; Silbey, R.; Bredas, J. L. Influence of interchain interactions on the absorption and luminescence of conjugated oligomers and polymers: A quantum-chemical characterization. *J. Am. Chem. Soc.* **1998**, *120*, 1289-1299.

(12) Shekhar, S.; Aharon, E.; Tian, N.; Galbrecht, F.; Scherf, U.; Holder, E.; Frey, G. L. Decoupling 2D Inter- and Intrachain Energy Transfer in Conjugated Polymers. *ChemPhysChem* **2009**, *10*, 576-581.

(13) Kim, Y.; Bouffard, J.; Kooi, S. E.; Swager, T. M. Highly emissive conjugated polymer excimers. *J. Am. Chem. Soc.* **2005**, *127*, 13726-13731.

(14) Kim, J.; Swager, T. M. Control of conformational and interpolymer effects in conjugated polymers. *Nature* **2001**, *411*, 1030-1034.

(15) Sun, Y. G.; Xia, Y. N. Shape-controlled synthesis of gold and silver nanoparticles. *Science* **2002**, *298*, 2176-2179.

(16) Yen, C. W.; Mahmoud, M. A.; El-Sayed, M. A. Photocatalysis in Gold Nanocage Nanoreactors. *J. Phys. Chem. A* **2009**, *113*, 4340-4345.

(17) Mahmoud, M. A.; El-Sayed, M. A. Comparative Study of the Assemblies and the Resulting Plasmon Fields of Langmuir-Blodgett Assembled Monolayers of Silver Nanocubes and Gold Nanocages. *J. Phys. Chem. C* **2008**, *112*, 14618-14625.

(18) Bryant, J., Georgia Institute of Technology, 2010.

(19) Liu, L. T.; Yaron, D.; Berg, M. A. Electron-phonon coupling in phenyleneethynylene oligomers: A nonlinear one-dimensional configuration-coordinate model. *J. Phys. Chem. C* **2007**, *111*, 5770-5782.

(20) Liu, L. T.; Yaron, D.; Sluch, M. I.; Berg, M. A. Modeling the effects of torsional disorder on the spectra of poly- and oligo-(p-phenyleneethynylenes). *J. Phys. Chem. B* **2006**, *110*, 18844-18852.

(21) Sluch, M. I.; Godt, A.; Bunz, U. H. F.; Berg, M. A. Excited-state dynamics of oligo(p-phenyleneethynylene): Quadratic coupling and torsional motions. *J. Am. Chem. Soc.* **2001**, *123*, 6447-6448.

(22) Wang, Y. Q.; Zappas, A. J.; Wilson, J. N.; Kim, I. B.; Solntsev, K. M.; Tolbert, L. M.; Bunz, U. H. F. Optical spectroscopy of grafted poly (p-phenyleneethynylene)s in water and Water-DMF mixtures. *Macromolecules* **2008**, *41*, 1112-1117.

(23) Bunz, U. H. F.; Imhof, J. M.; Bly, R. K.; Bangcuyo, C. G.; Rozanski, L.; Bout, D. A. V. Photophysics of poly [p-(2,5-didodecylphenylene)ethynylene] in thin films. *Macromolecules* **2005**, *38*, 5892-5896.

(24) Miteva, T.; Palmer, L.; Kloppenburg, L.; Neher, D.; Bunz, U. H. F. Interplay of thermochromicity and liquid crystalline behavior in poly(p-phenyleneethynylene)s: pi-pi interactions or planarization of the conjugated backbone? *Macromolecules* **2000**, *33*, 652-654.

(25) Jakubiak, R.; Collison, C. J.; Wan, W. C.; Rothberg, L. J.; Hsieh, B. R. Aggregation quenching of luminescence in electroluminescent conjugated polymers. *J. Phys. Chem. A* **1999**, *103*, 2394-2398.

(26) Ohira, A.; Swager, T. M. Ordering of poly(p-phenylene ethynylene)s in liquid crystals. *Macromolecules* **2007**, *40*, 19-25.

(27) Link, S.; El-Sayed, M. A. Shape and size dependence of radiative, non-radiative and photothermal properties of gold nanocrystals. *Int. Rev. Phys. Chem.* **2000**, *19*, 409-453.

(28) Kerker, M. The Optics of Colloidal Silver: Somethign Old and Something New. *J. Colloid Interface Sci.* **1985**, *105*, 297-314.

APPENDIX A

AGNC ARRAY CHARACTERIZATION AND PPE FLUORESCENT POLYMER SYNTHESIS IN CHAPTER 4

A.1 Additional Nanoparticle Characterization

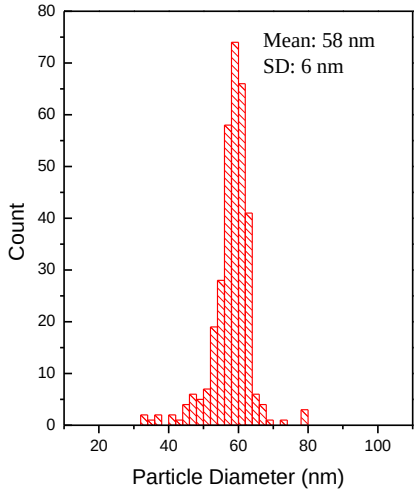

Figure A.1: Histogram indicating the size distribution of the silver nanocubes used; average size is 58 ± 6 nm.

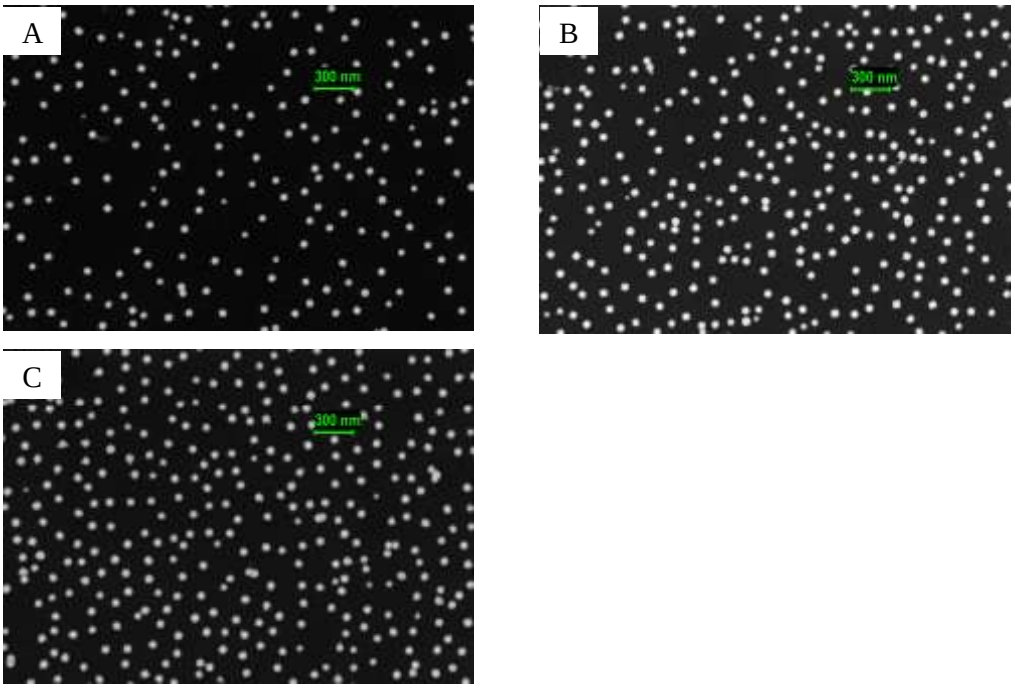

Figure A.2: SEM images of PVP capped AgNC monolayers that have been assembled on silicon substrates pressures of 0.5, 3, and 5 mN/m (A-C), which correspond to of 6.5, 10.1, and 11.2% surface coverage, respectively.

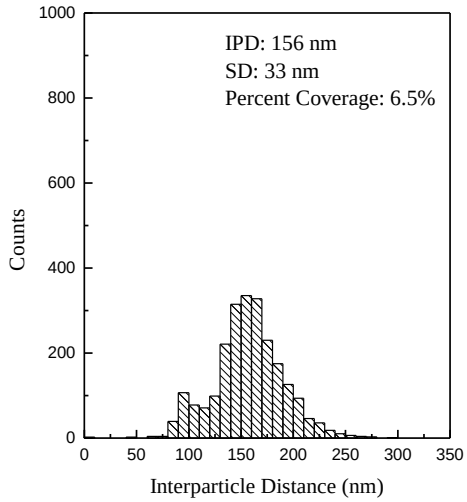

Figure A.3: Histogram indicating the average center-to-center distance between the silver nanocubes (nearest neighbor) at 6.5% surface coverage (omitted from Figure 4.3).

A.2 Synthesis of Poly(paraphenyleneethynylene) Fluorescent Polymer

A.2.1 Materials and Methods

All chemicals and solvents were purchased from commercial sources and were used without further purification unless otherwise specified. ^{1}H NMR spectra were recorded at 298 K on a 300 MHz spectrometer and chemical shifts are reported in parts per million (ppm), using residual solvent ($CDCl_3$ or D_2O) as an internal standard. The data is reported as follows: chemical shift, multiplicity (s = singlet, t = triplet, m = multiplet, br = broad), and integration. ^{13}C NMR spectra were recorded at 300 MHz, and ^{13}C chemical shifts (δ) are referenced to residual solvent ($CHCl_3$ or D_2O). Gel permeation chromatography data (vs. polystyrene standards in chloroform) was collected on a Shimadzu LC-10AT chromatographer (column length: 300 mm, diameter: 7.8 mm). Monomers **1** and **2** were synthesized according to published literature.[1-2]

A.2.2 Synthesis of Polymer 3

Monomer **1** (0.534 g, 1 mmol), Monomer **2** (0.451 g, 1 mmol), Dry THF (10 mL), and TEA (5 mL) were added to a 25 mL Schlenk tube and freeze, pump, thawed (3x). After removal of O_2, $(PPh_3)_2PdCl_2$ (0.5 mol%) and CuI (1 mol%) were added under N_2 and stirred at room temperature for 24 h. Upon completion of reaction, solution was precipitated in hexane (500 mL), filtered, and dried resulting in an orange powder (509 mg, 0.698 mmol, 70 %). GPC (vs. polystyrene standards in chloroform): M_n = 10840, M_w/M_n = 1.947, n = 15. ^{1}H NMR (300 MHz, $CDCl_3$): δ 7.12 (s, 2H), 7.03 (s, 2H), 4.89 (s, 4H), 4.29 (br, 4H), 4.20 (t, 4H), 3.85 (m, 4H), 3.82-3.75 (m, 4H), 3.70-3.65 (m, 8H), 3.57-3.52 (m, 4H), 3.44 (s, 6H) 1.22 (br, 6H). ^{13}C NMR (300 MHz, $CDCl_3$): δ 166.42, 151.31, 150.96, 118.21, 117.39, 113.39, 111.48, 91.53, 90.33, 70.85, 70.27, 69.87, 69.68, 68.63, 68.48, 67.98, 59.27, 58.46, 14.54.

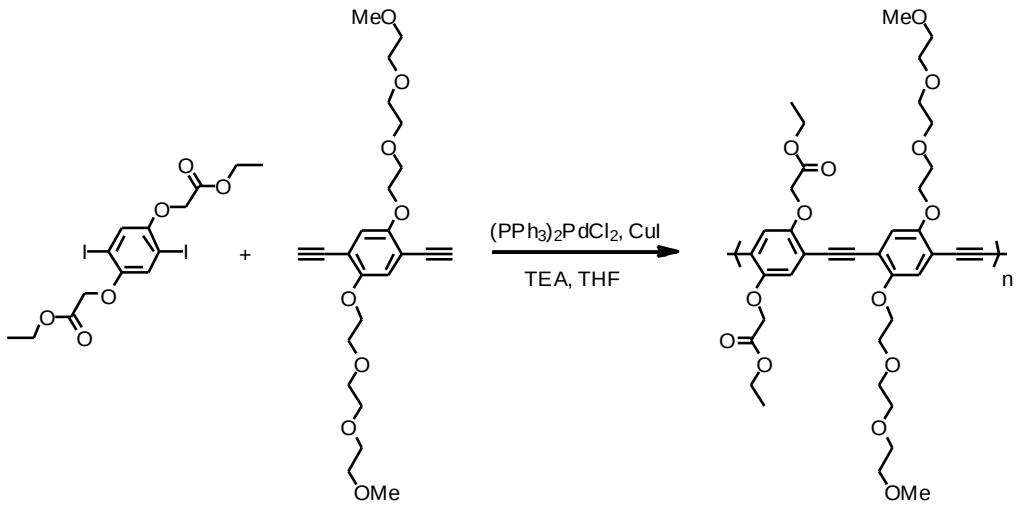

Figure A.4: Synthesis of Polymer 3 building blocks 1 and 2

A.2.3 Synthesis of Polymer 4

Polymer **3** (400 mg, 0.55 mmol) was dissolved in unsym-dimethylethylene-diamine (50 mL) and reacted at 50°C for 24 h. Upon completion of reaction, the solvent was removed and the polymer was washed with hexane, filtered, and dried resulting in an orange solid (397 mg, 0.487 mmol, 89%). ^{1}H NMR (300 MHz, $CDCl_3$): δ 7.16 (s, 2H), 7.05 (s, 2H), 4.48 (s, 4H), 4.24 (t, 4H), 3.83 (m, 4H), 3.79 – 3.73 (m, 4H), 3.69 – 3.63 (m, 8H), 3.58 – 3.50 (m, 4H), 3.47 (s, 6H), 3.39 (s, 4H), 2,80 (s, 4H), 2.23 (s, 12H). ^{13}C NMR (300 MHz, $CDCl_3$): δ 167.84, 159.54, 150.54, 119.31, 118.03, 112.25, 111.09, 91.39, 90.58, 70.48, 69.92, 69.43, 68.87, 68.23, 68.05, 67.87, 58.49, 57.93, 45.03, 37.27.

A.2.4 Synthesis of Polymer 5.

Polymer **4** (350 mg, 0.429 mmol) was dissolved in CH_2Cl_2 (50 mL) and CH_3I (25 mL) and reacted at room temperature overnight. Upon completion of reaction, the solvent was removed, and the polymer was dissolved in H_2O and dialyzed against DI H_2O (1 d), NaCl solution (1 d), and DI H_2O. After dialysis, the polymer solution was lyophilized resulting in a dark orange solid (297 mg, 0.325 mmol, 76%). ^{1}H NMR (300 MHz, D_2O): δ 7.11 (s, 2H), 7.05 (s, 2H), 4.18 (t, 4H), 4.53 (s, 4H), 3.89 (m, 4H), 3.84 – 3.79 (m, 4H), 3.74 (s, 4H), 3.69 – 3.61 (m, 8H), 3.54 – 3.48 (m, 4H), 3.42 (s, 10H), 3.23 (s, 18H). ^{13}C NMR (300 MHz, D_2O): δ 167.23, 157.65, 151.25, 119.61, 118.87, 114.08, 111.15, 92.97, 90.57, 70.23, 69.87, 69.54, 68.97, 68.63, 68.06, 65.89, 65.18, 59.47, 53.16, 36.51.

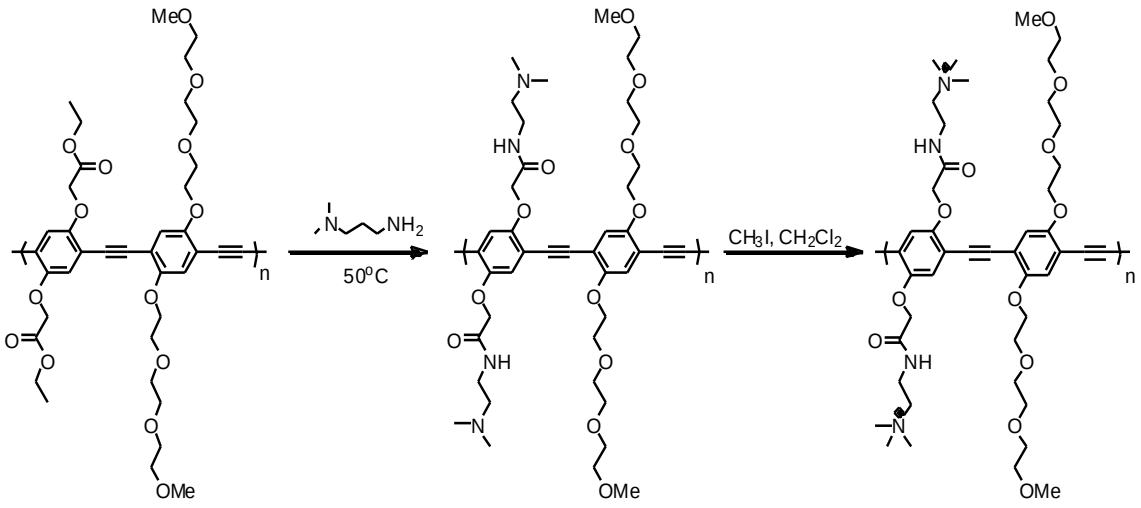

Polymer 3 **Polymer 4** **Polymer 5**

Figure A.5: Synthesis of Polymer 4 to obtain Polymer 5, which was ultimately used in this thesis

APPENDIX B

PPE FLUORESCENT POLYMER SOLUTION SPECTRA AND AGNC ARRAY IMAGES IN CHAPTER 5

B.1 Solution Spectra of PPE Fluorescent Polymer in Chloroform and Water

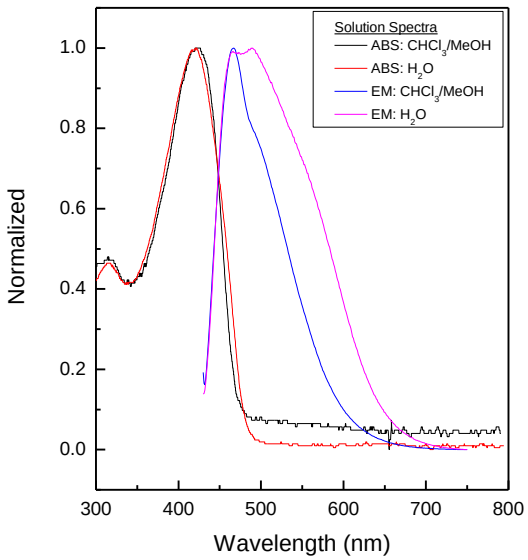

Figure B.1: The overlay PPE15 in $CHCl_3$/MeOH and H_2O are shown for comparison. The measurements illustrate the established solution-based effects of inter-chain interactions, via aggregation in H_2O.

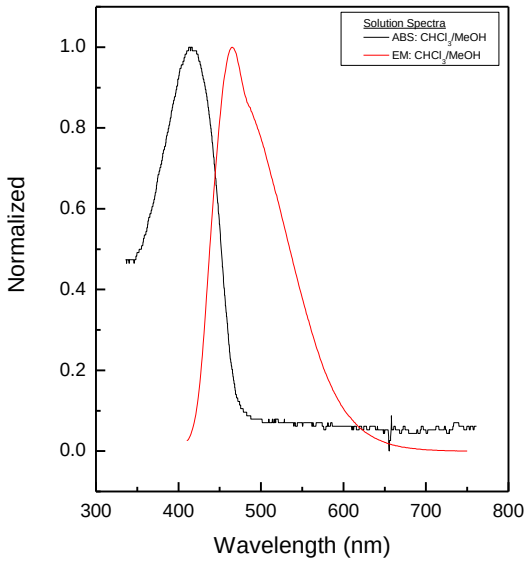

Figure B.2: The overlay of PPE25 in $CHCl_3$/MeOH (H_2O insoluble) is shown for comparison. Interestingly, the peak-shape of the solution based measurement does not match the spectral structure of the film, as is the case with PPE15. PPE25 is affected by the substrate to a much greater degree than the other polymers.

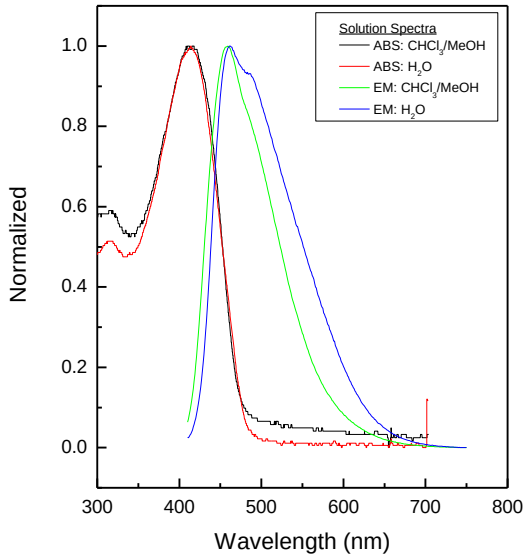

Figure B.3: The overlay PPE36 in $CHCl_3$/MeOH and H_2O are shown for comparison. Like PPE25, the peak-shape of the solution based measurement does not match the spectral structure of the film, as is the case with PPE15.

B.2 SEM Images of AgNC Arrays

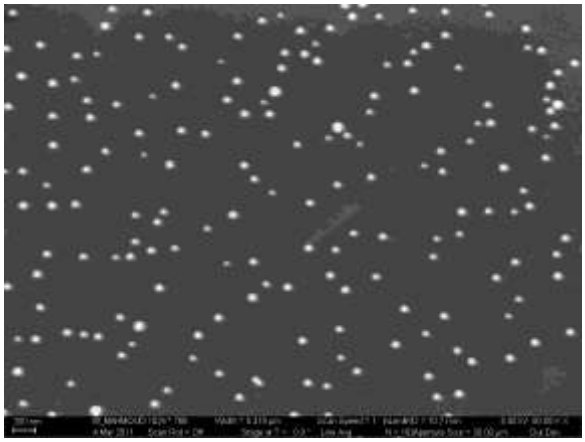

Figure B.4: AgNC monolayer at surface pressure of 0.0 mN/m.

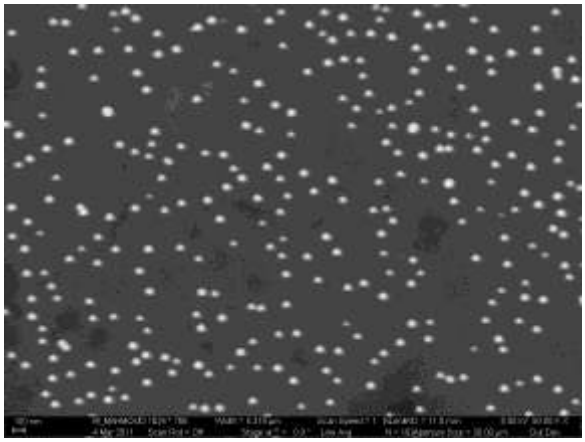

Figure B.5: AgNC monolayer at surface pressure of 0.2 mN/m.

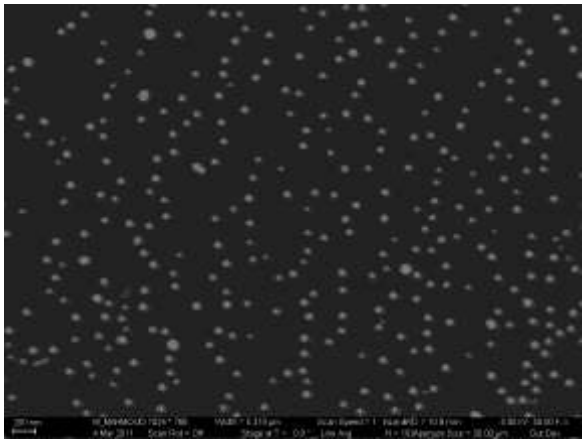

Figure B.6: AgNC monolayer at surface pressure of 0.5 mN/m.

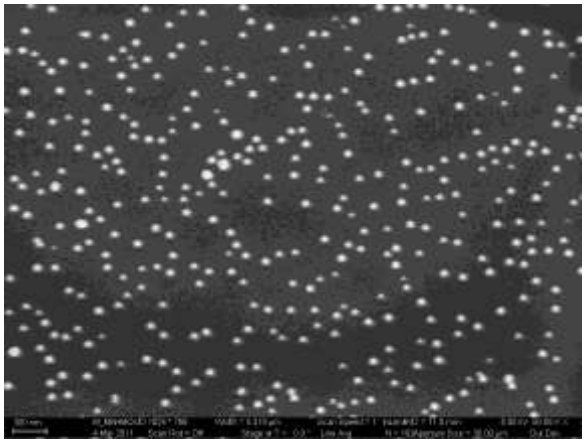

Figure B.7: AgNC monolayer at surface pressure of 1.0 mN/m.

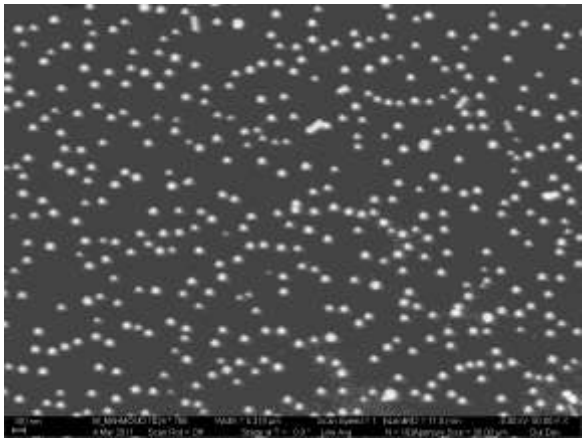

Figure B.8: AgNC monolayer at surface pressure of 3.0 mN/m.

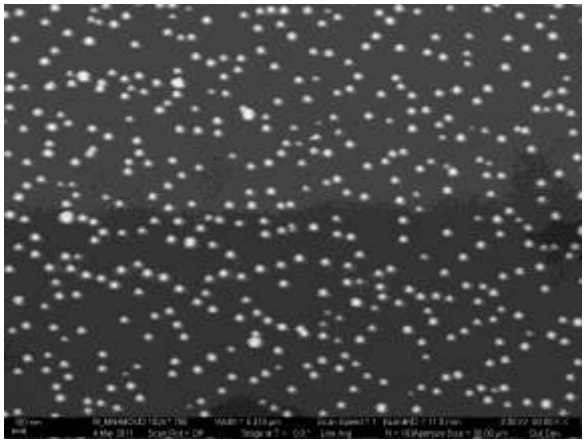

Figure B.9: AgNC monolayer at surface pressure of 5.0 mN/m.

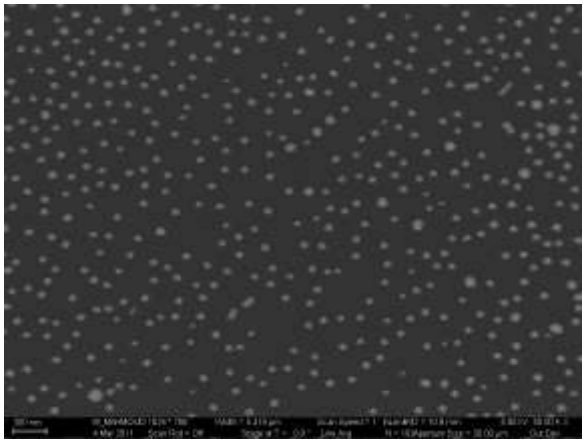

Figure B.10: AgNC monolayer at surface pressure of 6.0 mN/m.

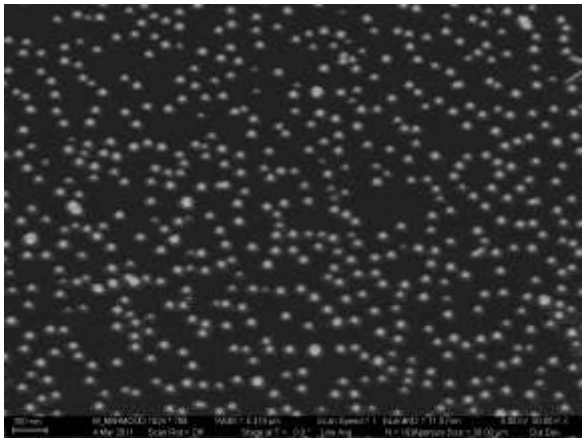

Figure B.11: AgNC monolayer at surface pressure of 8.0 mN/m.

B.3 Additional Extinction Spectra for AgNC-PPE 25 and 36

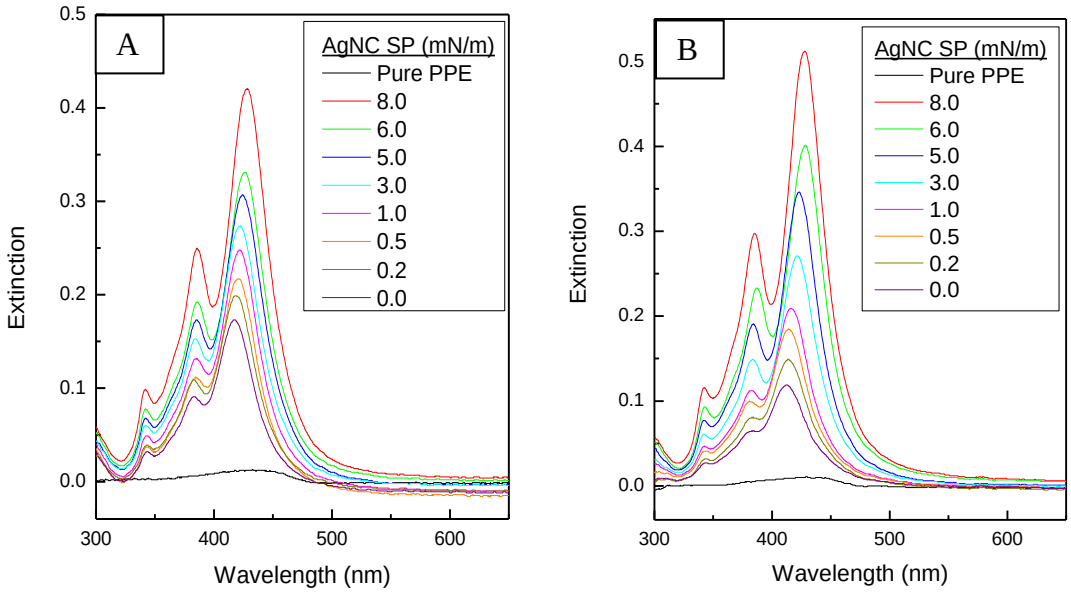

Figure B.12: Extinction spectra of (A) PPE25 and (B) PPE36. The optical density increases with increasing AgNC surface pressure from 0.0 to 8.0 mN/m.